

(shown with white arrows in Fig. 6A), suggesting little endogenous  $\alpha$ -synuclein was expressed in PC12 Tet-Off cells.

ATP-induced currents in  $\alpha$ -synuclein-transfected cells were not significantly different from those in mock-transfected cells (Fig. 6B). The relative amplitude of ATP-induced currents were  $28.6 \pm 4.1$  pA/pF ( $n = 9$ ) in mock-transfected cells and  $21.5 \pm 5.4$  pA/pF ( $n = 10$ ) in  $\alpha$ -synuclein-transfected cells, respectively.

#### Effects of kinase inhibitors on ATP-induced currents in parkin-transfected cells

The mechanism by which ATP-induced currents were augmented in parkin-transfected cells was investigated. It was reported that in *Aplysia* UCH activated PKA as a result of degradation of the regulatory subunit of PKA, and that this contributed to the long-term potentiation (Hegde et al., 1997). The increase of the ATP-induced inward currents in UCH-L1-transfected cells has also been attributed to activation of PKA (Manago et al., 2005). Therefore, it was tested whether PKA might be activated in parkin-transfected cells by using H-89, a PKA inhibitor. After obtaining large ATP-induced currents in parkin-transfected cells, 10  $\mu$ M H-89 was applied for 10 min. The amplitude of the ATP-induced currents in the presence of H-89 was  $64.6 \pm 3.5\%$  ( $n = 7$ ) of that of the first ATP-induced current in the same cell (control without H-89;  $85.3 \pm 4.0\%$  ( $n = 4$ )) (Fig. 7A), implying an inhibition of about 25%. An inactive analog of H-89, H-85, did not have this inhibitory effect (current amplitude in the presence of H-85 was  $84.3 \pm 1.6\%$  ( $n = 3$ ) of the first current). To confirm the effect of parkin, the effect of PKA inhibitor on ATP-induced currents were tested in mock-transfected cells as well. In mock-transfected cells, application of 10  $\mu$ M H-89 for 10 min had no effect on the ATP-induced inward current (H-89,  $79.8 \pm 1.4\%$  ( $n = 3$ ); control;  $77.6 \pm 5.2\%$  ( $n = 3$ )) (Fig. 7B).

The intracellular carboxyl terminus of P2X receptor contains several consensus phosphorylation sites for protein kinase C (PKC) as well as PKA, suggesting that the function of the P2X receptors might be regulated by PKC-mediated phosphorylation (Chow and Wang, 1998). Hence, the effect of chelerythrine, a PKC inhibitor, on ATP-induced currents in parkin-transfected

cells was tested. Application of 5  $\mu$ M chelerythrine for 10 min had no effect on the ATP-induced inward current in wild-type parkin-transfected cells (Fig. 7A). The normalized amplitude of second ATP-induced inward currents in the presence of chelerythrine was  $88.4 \pm 3.3\%$  ( $n = 5$ ). The possible involvement of calmodulin-dependent protein kinase (CaMKII) was also tested by using KN-93, a CaMKII inhibitor. Application of 10  $\mu$ M KN-93 for 20 min had no effect on the ATP-induced inward current in wild-type parkin-transfected cell ( $90.4 \pm 5.1\%$  ( $n = 4$ ); control,  $81.2 \pm 4.6\%$  ( $n = 4$ )) (Fig. 7C).

In PC12 cells and hippocampal neurons, activation of PKA has been reported to cause activation of extracellular signal-regulated kinase (ERK), with subsequent phosphorylation of  $\text{Ca}^{2+}$ -stimulated cAMP response element binding protein (CREB) and stimulated transcription (Impey et al., 1998). Likewise, the augmentation of ATP response in parkin-transfected cell might be due to the stimulation of transcription. To test this possibility, we examined whether mitogen-activated protein kinase (MAPK), including ERK, was activated following the activation of PKA in PC12 Tet-Off cells. However, ATP-induced currents in parkin-transfected cells were unaffected even after application of 5  $\mu$ M PD98059, (one of the MAPK kinase inhibitors) for 4 days: the amplitude of the ATP-induced current after the application of PD98059 was  $82.1 \pm 9.9$  pA/pF ( $n = 4$ ) compared with  $74.6 \pm 3.4$  pA/pF ( $n = 18$ ) in controls treated with vehicle (Fig. 7D).

#### Involvement of DARPP-32 in parkin-transfected PC12 Tet-Off cells

It was previously reported that the dopamine and cAMP-regulated phosphoprotein with molecular weight of about 32,000 (DARPP-32) was expressed in PC12 Tet-Off cells and that the expression level tended to increase after differentiation of the cells with NGF (Manago et al., 2005). Since phosphorylation of DARPP-32 at Thr-75 by cyclin-dependent kinase 5 (CDK5) had a negative feedback regulatory effect on PKA activity (Nishi et al., 2000), the effect of roscovitine, a CDK5 inhibitor, was tested. The application of 10  $\mu$ M roscovitine to wild-type parkin-expressing cells for 10 min enhanced the normalized amplitude of ATP-induced currents to the one

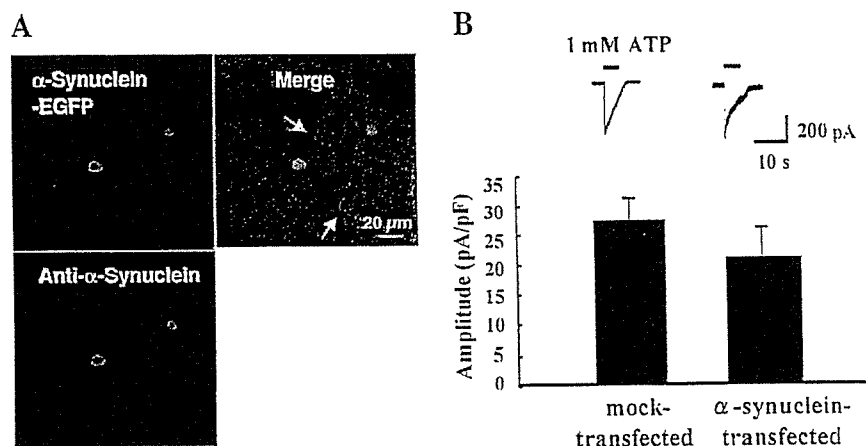


Fig. 6. The wild-type  $\alpha$ -synuclein-transfection had no effect on ATP-induced currents. A:  $\alpha$ -synuclein-transfected cells (EGFP; green) were strongly stained with anti- $\alpha$ -synuclein (red), while non-transfected cells (with arrows) were not. B: The amplitude of ATP-induced inward currents in mock and  $\alpha$ -synuclein-transfected cells.

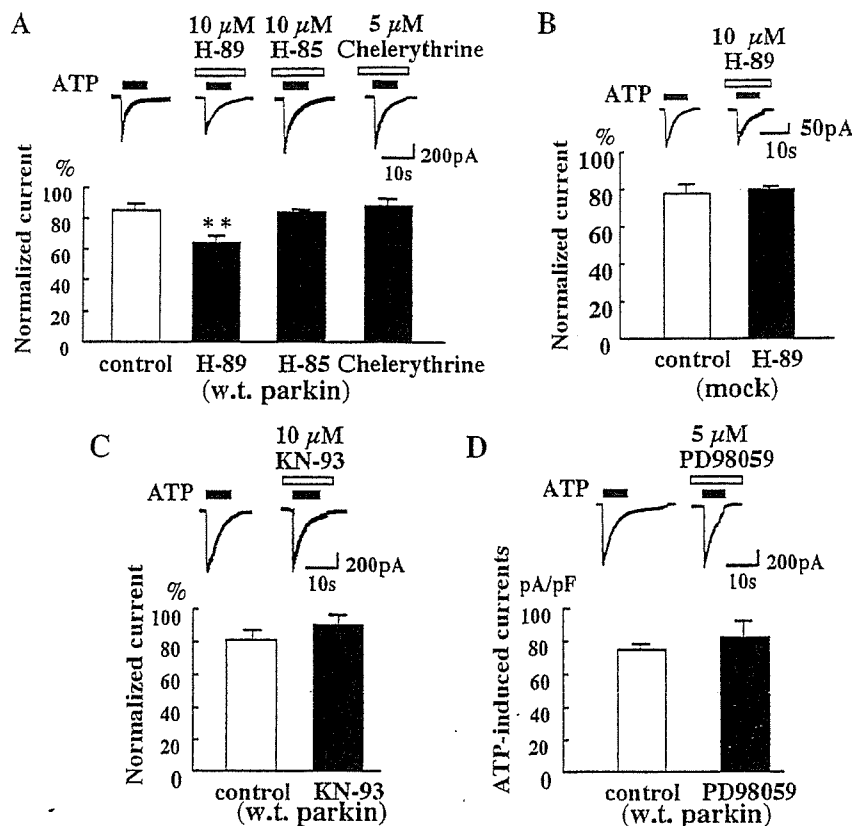


Fig. 7. Effects of kinase inhibitors on ATP-induced currents. A: In wild-type parkin-transfected cells, ATP-induced currents were attenuated by pre-application of 10  $\mu$ M H-89, a PKA inhibitor, but not either by 10  $\mu$ M H-85, an inactive analog of H-89, or 5  $\mu$ M chelerythrine, a PKC inhibitor, for 10 min. B: H-89 had no effect on

ATP-currents in control (mock-transfected) cells. C, D: In wild-type parkin-transfected cells, ATP-induced currents were not affected by application of 10  $\mu$ M KN-93, a CaMKII inhibitor, for 20 min (C), or by treatment with 5  $\mu$ M PD98059, a MAPKK inhibitor, for 4 days during differentiation (D). \*\* $P < 0.01$ .

before application of roscovitine ( $102.1 \pm 3.5\%$  ( $n = 4$ ); control without roscovitine;  $85.3 \pm 4.0\%$  ( $n = 4$ )) (Fig. 8A). The result suggested that PKA activity in parkin-transfected cells was negatively regulated by the phosphorylation of DARPP-32 at Thr-75 by CDK5.

Activation of PKA also influenced on protein phosphatases relating to DARPP-32 (Nishi et al., 2000). The phosphorylation of DARPP-32 at Thr-34 has been reported to inhibit protein phosphatase-1 (PP-1), leading to an apparent increase in substrate-phosphorylation. On the other hand, PKA activates protein phosphatase-2A (PP-2A), causing dephosphorylation of DARPP-32 at Thr-75, activating PKA in turn. To investigate the role of PP-1 and PP-2A in parkin-transfected cells, we applied 100 nM okadaic acid, an inhibitor for both PP-1 and PP-2A, for 20 min. The normalized currents were augmented to  $98.7 \pm 4.5\%$  ( $n = 5$ ) (control without okadaic acid;  $81.2 \pm 4.6\%$  ( $n = 4$ )) (Fig. 8B). These results suggested that the function of PP-1 was superior to that of PP-2A in parkin-transfected cells.

The effects of CDK5 inhibitor and okadaic acid on ATP-induced currents were tested in mock-transfected cells as well. In mock-transfected cells, application of 10  $\mu$ M roscovitine for 10 min had no effect on the ATP-induced inward current (roscovitine,  $82.5 \pm 5.2\%$  ( $n = 3$ ); control;  $77.6 \pm 5.2\%$  ( $n = 3$ )) (Fig. 8C). Similarly, application of 100 nM okadaic acid for 20 min did not affect the ATP-induced currents in mock-transfected cells, ( $76.5 \pm 3.5\%$  ( $n = 3$ ); control;  $80.0 \pm 4.7\%$  ( $n = 3$ )) (Fig. 8D).

#### Phosphorylation of DARPP-32 in parkin-transfected PC12 Tet-Off cells

To investigate whether or not the phosphorylation of DARPP-32 at Thr-34 or Thr-75 was modified by parkin, cells were immunostained using specific antibodies for DARPP-32 (phospho Thr-34 or phospho Thr-75). The staining of phospho Thr-34 in parkin-transfected cells were not enhanced as expected from the activation of PKA (Nishi et al., 2000) but rather attenuated (Fig. 9A). While phospho Thr-75 looked similar between parkin-transfected cell and non-transfected cells in the same field (Fig. 9B).

#### DISCUSSION

To understand the functional role of parkin in the central nervous system (CNS), it is important to know whether parkin has any effects on ion channels and receptors that are the basic elements of neurotransmission. To test this, we used PC12 cells and overexpressed parkin protein (Fig. 1A). These show well-developed inward current response to stimulation of P2X receptors by ATP (Nakazawa et al., 1994) and we recently reported enhancement of these currents by ubiquitin C-terminal hydrolase L1 (UCH-L1) (Manago et al., 2005). In the present experiments, we have studied the effects of overexpressing of parkin on these currents.

Parkin produced a very substantial increase in the maximum ATP-induced current without significant change in sensitivity to ATP (Figs. 1 and 3). This did not appear to be due to an increased number of P2X<sub>2</sub>,

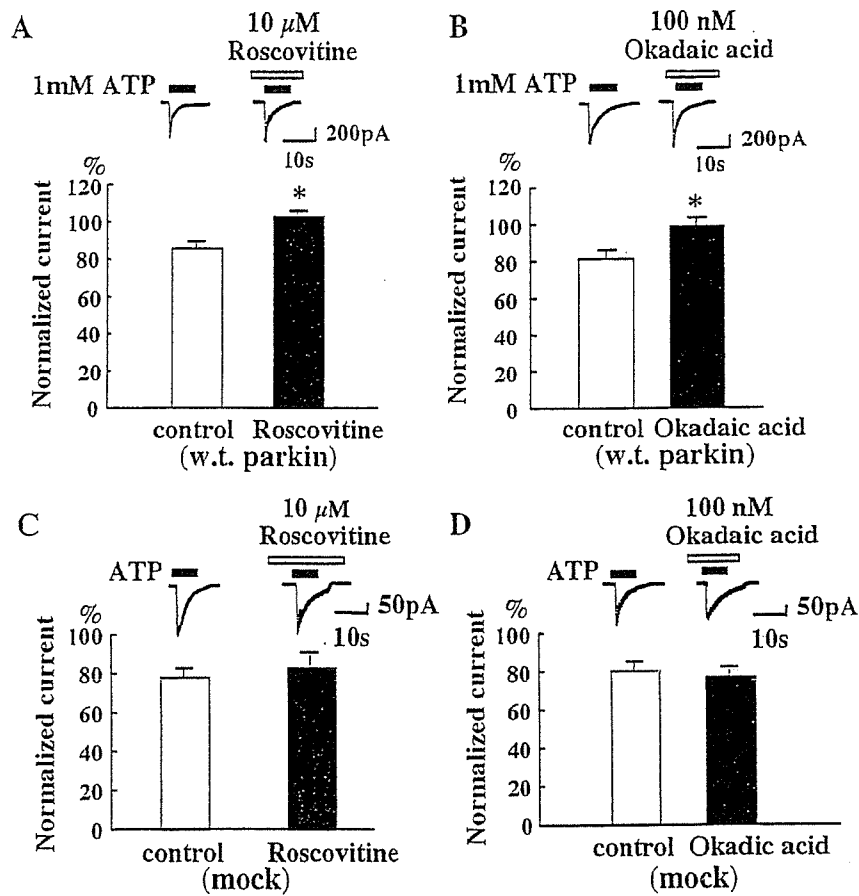


Fig. 8. Involvement of DARPP-32-related protein kinase and protein phosphatase on ATP-induced currents. In wild-type parkin-transfected cells, ATP-induced currents were augmented by pre-application of roscovitine, a CDK5 inhibitor, for 10 min (A) or 100 nM okadaic acid, a protein phosphatase inhibitor, for 20 min (B). In mock-transfected cells, ATP-induced currents were not affected by 10  $\mu$ M roscovitine (C) or 100 nM okadaic acid (D). \*\* $P < 0.05$ .

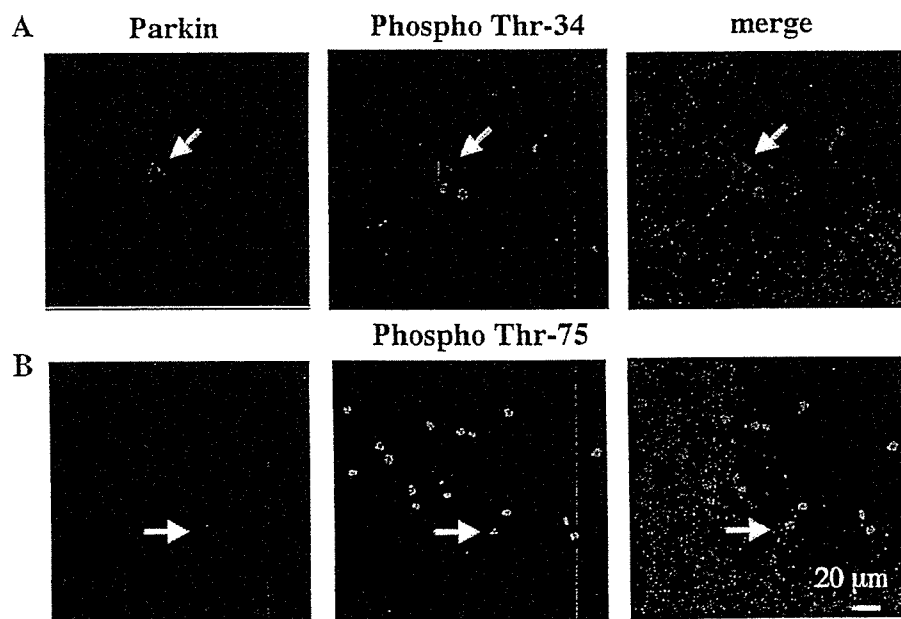


Fig. 9. Parkin did not increase the phosphorylation of DARPP-32. A: Immunostaining of phospho Thr-34 (red) looked rather smaller in parkin-transfected cell (yellow-green; white arrow). B: Immunostaining of phospho Thr-75 (red) looked similar between parkin-transfected cell (white arrow) and non-transfected cells. The merged images also include differential interference contrast images.

P2X<sub>4</sub>, or P2X<sub>6</sub> receptors, as judged by immunocytochemistry (Fig. 4). Therefore, the mechanism seems to involve an increase in gating of the receptors, rather than increased affinity or receptor number. Enhancement of P2X receptor at presynaptic terminal could increase neurotransmitter release; it was reported that ischemia-induced facilitation of glutamate release was due to the activation of P2X receptors in spiny neuron in neostriatum (Zhang et al., 2006) and our preliminary result showed that ATP increased the frequency of miniature inhibitory postsynaptic potential (mIPSP) in acutely isolated neuron from substantia nigra, suggesting increased release of GABA from presynaptic terminal (unpublished data).

The enhancement of ATP-induced currents seemed to be associated with the ubiquitin ligase activity of parkin since it was not reproduced by a ligase-deficient mutant (Figs. 2C and 3). Involvement of the ubiquitin–proteasome system would accord with our previous observations with the ubiquitin hydrolase UCH-L1, though in this case hydrolase activity itself was not required since the effect of UCH-L1 was replicated by a hydrolase-deficient construct. Instead, upregulation of mono-ubiquitin (Osaka et al., 2003) and ubiquitin ligase activity of UCH-L1 (Liu et al., 2002) might be responsible for the potentiation of ATP-induced currents.

Though the precise mechanism how ubiquitin ligase activity of parkin is involved is not known yet, possible signaling leading to enhancement of the ATP-induced currents is summarized in Fig. 10. It is only a part of the mechanism revealed in the present investigation, because inhibition of PKA, CDK5 or phosphatases resulted in only partial ( $\pm 20\%$ ) inhibition of the parkin-potentiated currents which showed threefold increase in amplitude compared to control.

At least, part of the increase in ATP-induced currents appeared to result from activation of PKA directly or indirectly, because PKA inhibitor partially attenuated parkin-induced potentiation of ATP-currents (Fig. 7A). In a reverse way, activation of PKA by forskolin augmented the ATP-induced currents in mock-transfected cells (Manago et al., 2005). One possible mechanism would be phosphorylation of P2X receptors by PKA. It was reported that activation of PKA potentiated ATP-evoked current in P2X<sub>4</sub>-transfected HEK293 cells (Brown et al., 2004), while there was an opposite result in P2X<sub>2</sub>-transfected HEK293 cells (Chow and Wang, 1998). CaMKII could be activated by PKA indirectly via an inhibition of PP-1 (Winder and Sweatt, 2001), but KN-93 did not have any effect on ATP-induced currents in parkin-transfected cells (Fig. 7C), suggesting that CaMKII was not significantly activated by parkin.

Since the enhancement was not completely reversed by inhibition of PKA, other mechanisms must be involved. One such mechanism might be through modification of DARPP-32. In rat striatum, it has been suggested that there is positive and negative feedback regulation of DARPP-32 via activation of PKA and CDK5, respectively (Nishi et al., 2000). Since DARPP-32 was expressed in PC12 cells (Manago et al., 2005), its possible involvement was tested using roscovitine, a CDK5 inhibitor, and okadaic acid, a protein phosphatase (PP-1 and PP-2A) inhibitor. Roscovitine further enhanced the ATP-induced currents in parkin-transfected cells (Fig. 8A), suggesting a negative-feedback role for CDK5. It seemed likely that parkin stimulated CDK5 since roscovitine did not have significant effect on mock-transfected cells (Fig. 8C). On the other hand, a role for phosphatases was suggested by the fact that okadaic acid further enhanced the ATP-induced

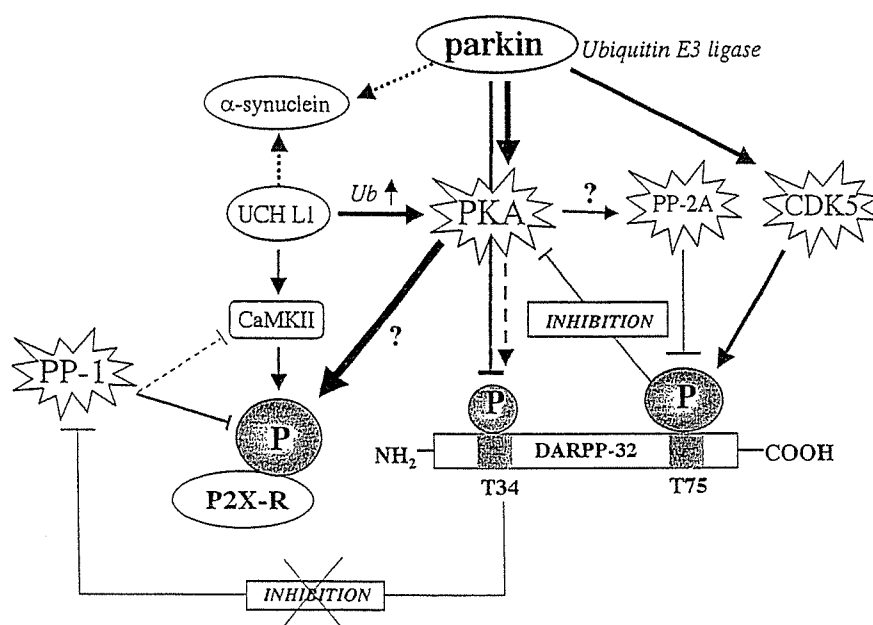


Fig. 10. Predicted signaling induced by expression of parkin. Parkin may activate PKA, subsequently phosphorylating P2X receptors. Parkin also may activate protein phosphatase-1 (PP-1) via inhibiting phosphorylation of DARPP-32 at Thr-34. On the other hand, phosphorylation and dephosphorylation of DARPP-32 at Thr-75 by CDK5 and PP-2A could compete with each other, keeping the level of phospho Thr-75 unchanged. As additional information, ubiquitin C-terminal hydrolase (UCH-L1) also activates PKA, which is independent on hydrolase activity but presumably due to the increase

in mono-ubiquitin level (Manago et al., 2005) or ubiquitin ligase activity (Liu et al., 2002). Unlike parkin, UCH-L1 activates Ca<sup>2+</sup> and calmodulin-dependent protein kinase (CaMKII), which could be indirectly activated by PKA and dephosphorylated by PP-1 (Winder and Sweatt, 2001). The effect of  $\alpha$ -synuclein, a substrate for both parkin and UCH-L1 (dotted line), was not clear, because transfection of  $\alpha$ -synuclein did not affect ATP-induced currents. Reported signaling but not confirmed in the present study was shown by dotted line.

currents in parkin-transfected cells (Fig. 8B). Since inhibition of PP-2A was supposed to inhibit PKA activity (Nishi et al., 2000; Manago et al., 2005), it seemed likely that this enhancement resulted mainly from inhibition of PP-1. In mock-transfected cells, okadaic acid did not have significant effect (Fig. 8D).

As for the phosphorylation of DARPP-32, activation of PKA would phosphorylate DARPP-32 at Thr-34 (Nishi et al., 2000). However, the staining of phospho Thr-34 was rather attenuated in parkin-transfected cells (Fig. 9A), suggesting that parkin may have inhibitory effect on the phosphorylation site at Thr-34. Therefore, parkin might indirectly activate PP-1, canceling the negative feedback from phospho Thr-34. Concerning the phosphorylation of DARPP-32 at Thr-75, CDK5, and PP-2A were supposed to have opposite effects, keeping the same level of phospho Thr-75 (Fig. 9B).

Both UCH-L1 and parkin can operate via  $\alpha$ -synuclein as a target substrate (Shimura et al., 2001; Snyder and Wolozin, 2004). It has recently been shown that UCH-L1, parkin, and  $\alpha$ -synuclein form lysine 63-linked multiubiquitin chains, which induce proteasomal-independent ubiquitination (Doss-Pepe et al., 2005; Lim et al., 2005). Therefore, it was possible that  $\alpha$ -synuclein also had potentiating effect on P2X receptors if lysine 63-linked multiubiquitin was involved. However,  $\alpha$ -synuclein did not have such effect (Fig. 6). It will be great interest to investigate the relationship between these three proteins and it may help to understand why parkin deficient-mice are not a robust model of parkinsonism (Perez and Palmiter, 2005), though there were alterations in energy metabolism, protein handling, and synaptic function (Periquet et al., 2005).

Another interesting point is that the signaling between activation of PKA and potentiation of P2X receptors induced by either UCH-L1 or parkin was not the same. For example, UCH-L1 but not parkin activated CaMKII and PP-2A whereas parkin but not UCH-L1 seemed to activate CDK5, producing a negative feedback effect on PKA (Fig. 10). In addition, we found that DARPP-32 (phospho Thr-34) was rather attenuated in spite of the report that activation of PKA increased the phosphorylation at Thr-34 (Nishi et al., 2000). The difference between UCH-L1 and parkin might due to the different substrate specificity as ubiquitin ligases.

Unfortunately, the low transfection efficiency precluded direct biochemical studies on the phosphorylation or dephosphorylation of specific proteins by parkin or UCH-L1. As a result, we have been restricted to pharmacological and immunocytochemical analyses. Nevertheless, the important point we have established is that enzymes working in the ubiquitin-proteasome system have clear and substantial effects on a neurotransmitter receptor and hence subsequently may affect neurotransmission in vivo. It is widely accepted that there are number of diseases related to aberrations in the ubiquitin system (Ciechanover and Schwartz, 2004), but how aberrations in the ubiquitin system cause neurodegenerative diseases such as Parkinson's disease (PD) is largely unknown. In the present study, one of the ubiquitin ligases, parkin, potentiated the function of P2X receptors, as well as another enzyme working in the ubiquitin-proteasome system, UCH-L1. Presynaptic P2X receptors triggers  $\text{Ca}^{2+}$ -dependent glutamate release in the brainstem (Shigetomi and Kato, 2004), though ATP-mediated inhibition of dopamine release was reported in rat neostriatum (Trendelenburg and Bultmann, 2000). It is of great interest how endogenous

parkin or UCH-L1 modulates neurotransmitter release by stimulating P2X receptors in vivo, which is now under investigation.

## ACKNOWLEDGMENTS

We thank Ms. Yuki Kosai for technical assistance to get confocal images and Prof. David A. Brown (University College London, UK) for reading the manuscript and giving many useful comments. Grants-in Aid for Scientific Research of Japan Society for Promotion of Science (No. 15082214), Grants-in Aid for Scientific Research in Priority Area Research of the Ministry of Education, Culture, Sports, Science and Technology, Japan (No. 16300126), Grants-in-Aid for Scientific Research of the Ministry of Health, Labour and Welfare, Japan (H15-Kokoro-023, H17-Genome-009) and a grant from the Program for Promotion of Fundamental Studies in Health Sciences of the National Institute of Biomedical Innovation (NIBIO), Japan (05-32).

## LITERATURE CITED

- Brown DA, Bruce JI, Straub SV, Yule DI. 2004. cAMP potentiates ATP-evoked calcium signaling in human parotid acinar cells. *J Biol Chem* 279:39485–39494.
- Chow YW, Wang HL. 1998. Functional modulation of P2X<sub>2</sub> receptors by cyclic AMP-dependent protein kinase. *J Neurochem* 70:2606–2612.
- Ciechanover A, Schwartz AL. 2004. The ubiquitin system: Pathogenesis of human diseases and drug targeting. *Biochim Biophys Acta* 1695:3–17.
- Cookson MR. 2005. The biochemistry of Parkinson's disease. *Annu Rev Biochem* 74:29–52.
- Doss-Pepe EW, Chen L, Madura K. 2005. Alpha-synuclein and parkin contribute to the assembly of ubiquitin lysine63-linked multiubiquitin chains. *J Biol Chem* 280:16619–16624.
- Hegde AN, Inokuchi K, Pei W, Casadio A, Ghirardi M, Chain DG, Martin KC, Kandel ER, Schwartz JH. 1997. Ubiquitin C-terminal hydrolase is an immediate-early gene essential for long-term facilitation in Aplysia. *Cell* 89:115–126.
- Hur EM, Park TJ, Kim KT. 2001. Coupling of L-type voltage-sensitive calcium channels to P2X<sub>2</sub> purinoceptors in PC-12 cells. *Am J Physiol Cell Physiol* 280:C1121–C1129.
- Huynh DP, Scoles DR, Nguyen D, Pulst SM. 2003. The autosomal recessive juvenile Parkinson disease gene product, parkin, interacts with and ubiquitinates synaptotagmin XI. *Hum Mol Genet* 12:2587–2597.
- Imai Y, Soda M, Takahashi R. 2000. Parkin suppresses unfolded protein stress-induced cell death through its E3 ubiquitin-protein ligase activity. *J Biol Chem* 275:35661–35664.
- Impey S, Obrietan K, Wong ST, Poser S, Yano S, Wayman G, Deloulme JC, Chan G, Storm DR. 1998. Cross talk between ERK and PKA is required for  $\text{Ca}^{2+}$  stimulation of CREB-dependent transcription and ERK nuclear translocation. *Neuron* 21:869–883.
- Kitada T, Asakawa S, Hattori N, Matsumine H, Yamamura Y, Minoshima S, Yokochi M, Mizuno Y, Shimizu N. 1998. Mutations in the parkin gene cause autosomal recessive juvenile parkinsonism. *Nature* 392:605–608.
- Ko HS, von Coelln R, Srivam SR, Kim SW, Chung KK, Pletnikova O, Troncoso J, Johnson B, Saffary R, Goh EL, Song H, Park BJ, Kim MJ, Kim S, Dawson VL, Dawson TM. 2005. Accumulation of the authentic parkin substrate aminoacyl-tRNA synthetase cofactor, p38/JTV-1, leads to catecholaminergic cell death. *J Neurosci* 25:7968–7978.
- Kubo S, Kitami T, Noda S, Shimura H, Uchiyama Y, Asakawa S, Minoshima S, Shimizu N, Mizuno Y, Hattori N. 2001. Parkin is associated with cellular vesicles. *J Neurochem* 78:42–54.
- Lim KL, Chew KC, Tan JM, Wang C, Chung KK, Zhang Y, Tanaka Y, Smith W, Engelder S, Ross CA, Dawson VL, Dawson TM. 2005. Parkin mediates nonclassical, proteasomal-independent ubiquitination of Synphilin-1: Implications for Lewy body formation. *J Neurosci* 25:2002–2009.
- Liu Y, Fallon L, Lashuel HA, Liu Z, Lansbury Jr. 2002. The UCH-L1 gene encodes two opposing enzymatic activities that affect alpha-synuclein degradation and Parkinson's disease susceptibility. *Cell* 111:209–218.
- Manago Y, Kanahori Y, Shimada A, Sato A, Amano T, Sato-Sano Y, Setsuie R, Sakurai M, Aoki S, Wang YL, Osaka H, Wada K, Noda M. 2005. Potentiation of ATP-induced currents due to the activation of P2X receptors by ubiquitin carboxy-terminal hydrolase L1. *J Neurochem* 92:1061–1072.
- Min BI, Kim CJ, Rhee JS, Akaike N. 1996. Modulation of glycine-induced chloride current in acutely dissociated rat periaqueductal gray neurons by l-opioid agonist DAGO. *Brain Res* 734:72–78.
- Nakazawa K, Inoue K. 1992. Roles of  $\text{Ca}^{2+}$  influx through ATP-activated channels in catecholamine release from pheochromocytoma PC12 cells. *J Neurophysiol* 68:2026–2032.
- Nakazawa K, Inoue K, Koizumi S, Inoue K. 1994. Facilitation by 5-hydroxytryptamine of ATP-activated current in rat pheochromocytoma cells. *Pflügers Arch* 427:492–499.
- Nishi A, Bibb JA, Snyder GL, Higashi H, Nairn AC, Greengard P. 2000. Amplification of dopaminergic signaling by a positive feedback loop. *Proc Natl Acad Sci USA* 97:12840–12845.
- Noda M, Nakanishi H, Nabekura J, Akaike N. 2000. AMPA-kainate subtypes of glutamate receptor in rat cerebral microglia. *J Neurosci* 20:251–258.
- Osaka H, Wang YL, Takada K, Takizawa S, Setsuie R, Li H, Sato Y, Nishikawa K, Sun YJ, Sakurai M, Harada T, Hara Y, Kimura I, Chiba S, Namikawa K, Kiyama H, Noda M, Aoki S, Wada K. 2003. Ubiquitin carboxy-terminal

- hydrolase L1 binds to and stabilizes monoubiquitin in neuron. *Hum Mol Genet* 12:1945–1958.
- Perez FA, Palmiter RD. 2005. Parkin-deficient mice are not a robust model of parkinsonism. *Proc Natl Acad Sci USA* 102:2174–2179.
- Periquet M, Corti O, Jacquier S, Brice A. 2005. Proteomic analysis of parkin knockout mice: Alterations in energy metabolism, protein handling and synaptic function. *J Neurochem* 95:1259–1276.
- Sela D, Ram E, Atlas D. 1991. ATP receptor. A putative receptor-operated channel in PC-12 cells. *J Biol Chem* 266:17990–17994.
- Shimura H, Hattori N, Kubo S, Mizuno Y, Asakawa S, Minoshima S, Shimizu N, Iwai K, Chiba T, Tanaka K, Suzuki T. 2000. Familial Parkinson disease gene product, parkin, is a ubiquitin-protein ligase. *Nat Genet* 25:302–305.
- Shimura H, Schlossmacher MG, Hattori N, Frosch MP, Trockenbacher A, Schneider R, Mizuno Y, Kosik KS, Selkoe DJ. 2001. Ubiquitination of a new form of alpha-synuclein by parkin from human brain: Implications for Parkinson's disease. *Science* 293:263–269.
- Snyder H, Wolozin B. 2004. Pathological proteins in Parkinson's disease: Focus on the proteasome. *J Mol Neurosci* 24:425–442.
- Shigetomi E, Kato F. 2004. Action potential-independent release of glutamate by  $Ca^{2+}$  entry through presynaptic P2X receptors elicits postsynaptic firing in the brainstem autonomic network. *J Neurosci* 24:3125–3135.
- Sriram SR, Li X, Ko HS, Chung KK, Wong E, Lim KL, Dawson VL, Dawson TM. 2005. Familial-associated mutations differentially disrupt the solubility, localization, binding and ubiquitination properties of parkin. *Hum Mol Genet* 14:2571–2586.
- Trendelenburg AU, Bultmann R. 2000. P2 receptor-mediated inhibition of dopamine release in rat neostriatum. *Neuroscience* 96:249–252.
- Winder DG, Sweatt JD. 2001. Roles of serine/threonine phosphatases in hippocampal synaptic plasticity. *Nat Rev Neurosci* 2:461–474.
- Zhang Y, Gao J, Chung KK, Huang H, Dawson VL, Dawson TM. 2000. Parkin functions as an E2-dependent ubiquitin-protein ligase and promotes the degradation of the synaptic vesicle-associated protein, CD97. *Proc Natl Acad Sci USA* 97:13354–13359.
- Zhang Y, Deng P, Li Y, Xu ZC. 2006. Enhancement of excitatory synaptic transmission in spiny neurons after transient forebrain ischemia. *J Neurophysiol* 95:1537–1544.

## Solo/Trio8, a Membrane-Associated Short Isoform of Trio, Modulates Endosome Dynamics and Neurite Elongation

Ying-Jie Sun,<sup>1,5†</sup> Kaori Nishikawa,<sup>1,3†</sup> Hideki Yuda,<sup>1</sup> Yu-Lai Wang,<sup>1</sup> Hitoshi Osaka,<sup>3</sup>  
Nobuna Fukazawa,<sup>1,4</sup> Akira Naito,<sup>5</sup> Yoshihisa Kudo,<sup>4</sup>  
Keiji Wada,<sup>1,7</sup> and Shunsuke Aoki<sup>1,2,6,7\*</sup>

Department of Degenerative Neurological Diseases<sup>1</sup> and Department of Demyelinating Disease and Aging,<sup>2</sup> National Institute of Neuroscience, NCNP, Kodaira, Tokyo 187-8502, Japan; Japan Science and Technology Agency (JST), Kawaguchi, Saitama 332-0012, Japan<sup>3</sup>; Laboratory of Cellular Neurobiology, Tokyo University of Pharmacology and Life Science, Hachioji, Tokyo 192-0392, Japan<sup>4</sup>; Department of Anatomy and Structural Science, Yamagata University School of Medicine, Yamagata 990-9585, Japan<sup>5</sup>; New Energy and Industrial Technology Development Organization (NEDO), Kawasaki, Kanagawa 212-8554, Japan<sup>6</sup>; and JST, CREST, Kawaguchi, Saitama 332-0012, Japan<sup>7</sup>

Received 28 December 2005/Returned for modification 15 February 2006/Accepted 28 June 2006

With DNA microarrays, we identified a gene, termed *Solo*, that is downregulated in the cerebellum of Purkinje cell degeneration mutant mice. *Solo* is a mouse homologue of rat *Trio8*—one of multiple *Trio* isoforms recently identified in rat brain. *Solo/Trio8* contains N-terminal sec14-like and spectrin-like repeat domains followed by a single guanine nucleotide exchange factor 1 (GEF1) domain, but it lacks the C-terminal GEF2, immunoglobulin-like, and kinase domains that are typical of *Trio*. *Solo/Trio8* is predominantly expressed in Purkinje neurons of the mouse brain, and expression begins following birth and increases during Purkinje neuron maturation. We identified a novel C-terminal membrane-anchoring domain in *Solo/Trio8* that is required for enhanced green fluorescent protein-*Solo/Trio8* localization to early endosomes (positive for both early-endosome antigen 1 [EEA1] and Rab5) in COS-7 cells and primary cultured neurons. *Solo/Trio8* overexpression in COS-7 cells augmented the EEA1-positive early-endosome pool, and this effect was abolished via mutation and inactivation of the GEF domain or deletion of the C-terminal membrane-anchoring domain. Moreover, primary cultured neurons transfected with *Solo/Trio8* showed increased neurite elongation that was dependent on these domains. These results suggest that *Solo/Trio8* acts as an early-endosome-specific upstream activator of Rho family GTPases for neurite elongation of developing Purkinje neurons.

Endosomal membrane trafficking in neurons plays a key role in various neural processes, including neurite elongation (19, 33), synaptic transmission (17), neuronal degeneration (36), and neuronal cell death or survival (7). The early endosome regulates the selective transfer of membrane proteins to other organelles, and thus it is a key organelle for sorting vesicles containing cell surface membrane proteins, including receptors, transporters, channels, and cell adhesion molecules (2, 29, 39, 47).

Several lines of evidence suggest that small GTPases play pivotal roles in regulating early-endosome dynamics (2, 39, 47). For example, Rab5 regulates the motility and fusion of early endosomes (32), whereas Rab4 and Rab5 control vesicle influx and efflux, respectively, in the early-endosome pool (28). Rho family GTPases also regulate early-endosome dynamics. Once such GTPase, Cdc42, controls endocytic transport in polarized cells (20), whereas RhoD specifically localizes to early endosomes and regulates their motility via diaphanous-related formin proteins (13). Upstream regulators of small GTPases that associate with early endosomes have been studied exten-

sively. For example, early-endosome antigen 1 (EEA1) acts as an effector for Rab family small GTPases (5, 45). Although Rho family GTPases are also activated by multivalent upstream effectors (42), the specialized upstream activators that function in early endosomes remain unknown.

*Trio*, a member of the Dbl homology domain family of guanine nucleotide exchange factors (GEFs), was originally identified by its interaction with the leukocyte common antigen-related protein receptor (6). *Trio* has an N-terminal sec14-like domain, spectrin-like repeats, two GEF domains (GEF1 and GEF2), an immunoglobulin (Ig)-like domain, and a C-terminal Ser/Thr kinase domain (3). The GEF1 domain activates RhoG and Rac1, whereas GEF2 acts on RhoA, suggesting that *Trio* is involved in multiple GTPase cascades mediating various cellular processes (3). Genetic analysis of the *Trio* gene in *Drosophila* embryos implicates this protein in neuronal and retinal axon guidance (3). Mice lacking *Trio* die during embryogenesis and exhibit a loss of myofiber formation and cellular disorganization in the hippocampus and olfactory bulb (35). Although *Trio* is highly expressed in the adult brain, heart, liver, skeletal muscle, kidney, placenta, and pancreas (6), its effector function in these adult tissues remains unknown. Several *Trio* isoforms were recently identified (25), and the expression of each isoform was shown to be regulated in a tissue-specific manner. The functions of these isoforms, however, have not been delineated.

Purkinje cell degeneration (pcd) is an autosomal recessive

\* Corresponding author. Mailing address: Department of Degenerative Neurological Diseases, National Institute of Neuroscience, National Center of Neurology and Psychiatry, 4-1-1 Ogawahigashi, Kodaira, Tokyo 187-8502, Japan. Phone: 81-42-346-1715. Fax: 81-42-346-1745. E-mail: aokis@ncnp.go.jp.

† Y.-J.S. and K.N. contributed equally to this work.

mutational disorder in mice that is characterized by degenerative loss of Purkinje neurons after postnatal day 15 (P15) to P18 (30). The causative mutation of *pcd* was identified at the *Nnal* locus (12). The disorder constitutes an adult-onset disease and presents mild phenotypes, thereby facilitating the analysis of cerebella that are nearly devoid of Purkinje neurons. Thus, the *pcd* mouse has been repeatedly used to screen for Purkinje neuron-specific genes, such as the gene encoding 28-kDa calbindin (34) or inositol 3-phosphate receptor 1 (IP3R) (24).

In this study, we used DNA microarrays to analyze gene expression in the cerebella of mice carrying a mutation governing *pcd* (30). We identified a Purkinje-predominant mouse cDNA encoding the protein Solo, which is a membrane-associated isoform of Trio. Amino acid sequence analysis showed that Solo is a homologue of the recently identified rat protein Trio8 (25). Solo/Trio8 specifically localized to early endosomes and regulated their dynamics. We also found that Solo/Trio8 modulated neurite morphology in primary cultured neurons. These data suggest that Solo/Trio8 is involved in the development of Purkinje neurons by affecting the dynamics of early endosomes.

#### MATERIALS AND METHODS

**Animals.** C57BL/6J-*pcd* mice were obtained from The Jackson Laboratory (Bar Harbor, ME). The cerebella of P24 *pcd* and wild-type (WT) mice were used for DNA microarrays. For SYBR green-based real-time quantitative reverse transcription (RT)-PCR, three cerebella were collected on each postnatal day. Animal care and handling were in accordance with institutional regulations for animal care and public law and were approved by the Animal Investigation Committee of the National Institute of Neuroscience, Japan.

**DNA microarrays.** Equivalent amounts of total RNA derived from each cerebellar sample were reverse transcribed into double-stranded cDNA that was then used as a template to synthesize biotin-labeled cRNA with the BioArray HighYield RNA transcription labeling kit (Enzo Diagnostics, Farmingdale, NY). Labeled cRNA was purified on RNeasy affinity resin (QIAGEN, Valencia, CA) and fragmented randomly to an average size of 50 to 100 bases by incubation in 40 mM Tris-acetate, pH 8.2, containing 100 mM K-acetate and 30 mM Mg-acetate at 94°C for 35 min. The labeled cRNA samples were analyzed with the Affymetrix murine genome U74A, -B, and -C array set (Affymetrix, Santa Clara, CA). Hybridization and array scanning were performed according to protocols provided by Affymetrix. Data analysis was performed with Microarray Suite software (Affymetrix).

**5' RACE.** 5' rapid amplification of cDNA ends (RACE) was performed with the 5' RACE kit (Invitrogen, Carlsbad, CA) according to the manufacturer's protocol. First-strand cDNA was synthesized from cerebellar total RNA with a gene-specific primer (5'-AGAAACCAAAATGAGGCTGCTA-3') corresponding to the cDNA sequence of expressed sequence tag (EST) clone A1587721. Nested PCR was performed to amplify DNA between the anchor primer and another primer (5'-TGAGGCTGCTAAGAATGGCTTGACTG-3') specific for A1587721. The product (~1.2 kbp) displayed strong homology to the Trio cDNA sequence (GenBank accession no. NM\_007118). A cDNA encoding the Solo/Trio8 open reading frame (ORF) was obtained by RT-PCR with primers 5'-TCTCGAGATGAAAGCTATGGATGTTTGGCC-3' and 5'-AGAATTCGAATGAAAGGTAAGGAACTGAG-3', derived from the human Trio gene (GenBank accession no. NM\_007118) and the 1.2-kbp product, respectively. The resulting 5.6-kbp Solo/Trio8 DNA fragment was subcloned into the pGEM-T Easy vector (Promega, Madison, WI) for further sequencing.

**In situ hybridization.** In situ hybridization was performed as described previously (1). To synthesize cRNA probes for the Trio gene, the 357-bp fragment encoding part of the Solo gene (nucleotides [nt] 5134 to 5490; DDBJ accession no. AB106872; common probe) and a 339-bp noncoding part of the Solo gene (nt 5606 to 5944; Solo-specific probe) were subcloned into pBluescript-SKII (+) (Stratagene, La Jolla, CA).

**SYBR green-based real-time quantitative RT-PCR.** SYBR green-based real-time quantitative RT-PCR was performed with primers 5'-TCTCTCAGACAGACAGCCACGT-3' (forward) and 5'-TGCTTCATATTAAGGGCAGCAG-3'

(reverse) to amplify Solo/Trio8 cDNA and primers 5'-AGAAGGTGGTGAAGCAGGCAT-3' (forward) and 5'-ATCGAAGGTGGAAGAGTGGGA-3' (reverse) for glyceraldehyde-3-phosphate dehydrogenase (GAPDH) cDNA. The quantitative RT-PCR method (user bulletin 2; Applied Biosystems, Foster City, CA) was modified to establish an expression level index for mRNA (1).

**Plasmid constructs.** With mouse cerebellar cDNA as a template, we performed PCR to construct plasmids encoding full-length (amino acids [aa] 1 to 1849) Solo/Trio8 tagged (N or C terminally) with enhanced green fluorescent protein (EGFP) and FLAG; Solo/Trio8 mutant constructs lacking the C-terminal transmembrane domain [Solo-TM(-)] aa 1 to 1830; DDBJ accession no. AB106872] were prepared similarly. The primers used were 5'-CCGCTCGAGATGAAAGCTATGGATGTTTGGCC-3' [forward primer for N- or C-terminally EGFP-tagged Solo and EGFP-Solo-TM(-)], 5'-GGAAATTCGAATGGAAGGTAAGGAACTGAGC-3' (reverse primer for EGFP-Solo), 5'-GGAAATTCGCTTGTTCATCTCGAGTCCGGCTGA-3' [reverse primer for EGFP-Solo-TM(-)], 5'-CCGCTCGAGCGATGGACTACAAGGACGACGATGACAAGATGAAAGCTATGGATGTTTGGCC-3' [forward primer for N-terminally FLAG-tagged Solo and FLAG-Solo-TM(-)], 5'-GGGGGCGGCCCTCAAATGGAAGGTAAGGAACT-3' (reverse primer for N-terminally FLAG-tagged Solo), 5'-GGGGGCGGCCGCTCACTTGTCTCCTGCGAGTCCG-3' [reverse primer for N-terminally FLAG-tagged Solo-TM(-)], 5'-CCGCTCGAGATGGAAGCTATGGATGTTTGGC-3' [forward primer for C-terminally FLAG-tagged Solo and FLAG-Solo-TM(-)], 5'-GGGGGCGGCCGCTTACTTGTCTCGTCTGCTTGTAGTCAATGGAAGGTAAGGTAAGTGAAGC-3' (reverse primer for C-terminally FLAG-tagged Solo), 5'-GGGGGCGGCCGCTTACTTGTCTCGTCTGCTTGTAGTCTTGTCTGCTCCTCGAGTCCGGCTG-3' [reverse primer for C-terminally FLAG-tagged Solo-TM(-)]. *Pfu* DNA polymerase was used for PCR, and the amplified products were cloned between the XhoI and EcoRI sites of pEGFP-C3/pEGFP-N1 (Clontech, Palo Alto, CA) or the XhoI and NotI sites of pCI-neo (Promega). To construct the GFP1-inactivated Solo mutant form Solo-AE, the mutations Gln<sup>1368</sup> to Ala and Leu<sup>1376</sup> to Glu were introduced into EGFP-Solo with the QuikChange site-directed mutagenesis kit (Stratagene) and primers 5'-CAAACAGTTGCCCGGATAACAAAGTATCAGCTCGAGTTAAAGGAG-3' and 5'-CTCCTTAACTCGAGCTGATACTTTGTTATCCGGGCAACTGGT TTG-3'. All gene constructs were confirmed by DNA sequencing. Expression of the genes for Solo/Trio8 was controlled with a cytomegalovirus promoter.

**Cell culture and transient transfections.** COS-7, HEK293T, and NIH 3T3 cells were cultured at 37°C in 5% CO<sub>2</sub> in Dulbecco modified Eagle medium containing 10% fetal bovine serum, 100 U/ml penicillin, and 85 µg/ml streptomycin (Invitrogen). Cells were grown on 6- and 24-well or 100-mm dishes and four- and eight-well chamber slides and transfected with equal amounts (0.4 to 3.0 or 20 µg) of plasmid DNA per well with the Lipofectamine 2000 DNA transfection reagent (Invitrogen) according to the manufacturer's instructions and cultured for 8 to 24 h at 37°C.

**Rac1 pull-down assay.** COS-7 cells were cultured at a density of  $2 \times 10^6$  cells per 100-mm dish and transfected with 20 µg of an EGFP-Solo expression construct or a control plasmid (pEGFP) as described above. After 16 h, cells were serum starved for 5 h and then washed with phosphate-buffered saline (PBS) and lysed in lysis buffer (25 mM HEPES, [pH 7.5], 150 mM NaCl, 1% [wt/vol] Igepal CA-630, 20 mM MgCl<sub>2</sub>, 1 mM EDTA, 2% [wt/vol] glycerol, 1 mM Na<sub>2</sub>VO<sub>4</sub>, 25 mM NaF, complete EDTA-free protease inhibitor mixture [Roche Molecular Biochemicals, Indianapolis, IN]). Cell lysates were centrifuged at 20,000 × g for 20 min at 4°C. Rac1 activation was measured with the Rac1 activation assay kit (Upstate Biotechnology Inc., Lake Placid, NY) according to the manufacturer's instructions. Briefly, 0.5 ml of the supernatant (2 mg protein) was added to 10 µl of PAK1-p21-binding domain (PBD)-glutathione S-transferase-glutathione agarose beads (Upstate Biotechnology, Inc.), and the mixture was rotated for 1 h at 4°C, followed by three washes of the protein complexes with lysis buffer. PAK1-PBD-bound proteins were dissociated and denatured by boiling in Laemmli sample buffer and subjected to sodium dodecyl sulfate-polyacrylamide gel electrophoresis. The amount of active Rac1 (GTP-bound form) was analyzed by immunoblotting with a monoclonal antibody to Rac1 (Upstate Biotechnology, Inc.).

**Cell fractionation.** COS-7 cells were transfected with expression plasmids and cultured for 24 h. The cells were homogenized in 300 µl of ice-cold TNE buffer (50 mM Tris-HCl [pH 7.5], 150 mM NaCl, 1 mM EDTA) supplemented with protease inhibitors (Complete Protease Inhibitors; Roche Molecular Biochemicals) and sonicated for 30 s on ice. The homogenates were subjected to centrifugation at 20,000 × g for 30 min at 4°C. Supernatants (cytoplasmic fraction) were pooled, and pellets (including light membranes) were washed twice with 0.5 ml of TNE buffer and then lysed for 30 min on ice in radioimmunoprecipitation assay buffer (50 mM Tris-HCl [pH 7.5], 150 mM NaCl, 1 mM EDTA, 0.5%



sodium deoxycholate, 0.1% sodium dodecyl sulfate) with protease inhibitors and subjected to centrifugation at  $20,000 \times g$  for 30 min at 4°C.

**Western blotting.** Western blotting was performed as described previously (1). Blots were probed with antibodies to detect EGFP (anti-Living Colors A.v., JL-8; Clontech), anti-FLAG M2 (Sigma, St. Louis, MO), anti-I $\kappa$ -B (Cell Signaling Technology, Beverly, MA), anti-platelet-derived growth factor (PDGF) receptor  $\alpha/\beta$  (Upstate Biotechnology, Inc.) or anti- $\beta$ -actin (Sigma).

**Neuronal cultures and transfections.** Fetal C57BL/6J mice at embryonic day 16 (E16) were used for the primary culture of embryonic cortical neurons. The brain of each embryo was dissected from the overlying meninges, blood vessels, olfactory bulb, and hippocampus in Hanks' balanced salt solution (HBSS; Gibco, Gaithersburg, MD). Brains were minced with a 0.1-mm blade, and small pieces of the tissues were incubated in 0.25% trypsin–0.04% EDTA (Gibco) for 10 min at 37°C. Digestion was stopped by addition of 2% fetal bovine serum, and the mixture was incubated with 0.01% DNase I (Sigma) at room temperature for 2 min. After being spun down (5 min at  $280 \times g$ ), neuronal cells were resuspended in HBSS. Single-cell suspensions were obtained by trituration and filtered through a 70- $\mu$ m nylon cell strainer (BD, Bedford, MA) to remove undigested cell aggregates, followed by centrifugation for 5 min at  $280 \times g$ . Dispersed neurons were plated on Biocoat poly-D-lysine-coated four-well chamber slides (BD) at a density of  $2 \times 10^5$  or  $4 \times 10^5$  cells per well in Neurobasal medium (Invitrogen) containing B27 supplement (Invitrogen), penicillin-streptomycin (Invitrogen), and 2 mM L-glutamine (Invitrogen). The cultures were maintained at 37°C in a 5% CO<sub>2</sub> humidified incubator, and half of the medium volume was replaced with fresh medium about every 2 days. Cortical neurons were grown for 6 days in culture and then transfected as described above. For cotransfections, Lipofectamine 2000 reagent (4  $\mu$ l) and DNA (a total of 1.6  $\mu$ g of plasmids containing EGFP or EGFP-fused protein and DsRed [pDsRed Express-C1; Clontech] at a ratio of 8:1) were separately suspended in Opti-MEM (50  $\mu$ l; Invitrogen) and gently combined. After a 20-min incubation at room temperature, the mixture (100  $\mu$ l) was added to the culture medium (400  $\mu$ l). DsRed is used to visualize the morphology of the transfected neurons (41). Neurons were allowed to express the transfected protein for 18 h, fixed with 4% formaldehyde in PBS, and immunostained with polyclonal anti-DsRed (1:10,000; rabbit IgG; BD) and mouse monoclonal anti-GFP 3E6 (1:2,000; Molecular Probes, Eugene, OR). Alexa Fluor dye-conjugated secondary antibodies (1:400; Molecular Probes) were used.

**Immunofluorescence microscopy.** Fluorescence immunostaining was performed as described previously (1). Dilutions of primary antibodies were as follows: anti-EEA1, anti-Bip/GRP78, and anti-GM130 (from BD Biosciences), all 1:100; anti-Rab5a and anti-Rab5b (Santa Cruz Biotech, Santa Cruz, CA), 1:200; anti-Rab7 (Santa Cruz Biotech), 1:100; anti-Tau1 and anti-Map2 (Chemicon International, Temecula, CA), 1:200; anti-calbindin D28k (Swant, Bellinzona, Switzerland), 1:500. All Alexa Fluor dye-conjugated secondary antibodies (Molecular Probes) were diluted 1:200. Immunofluorescence microscopy was performed with an ORCA-ER digital camera (Hamamatsu Photonics, Hamamatsu, Japan), and confocal microscopy was performed with the FLUOVIEW system (Olympus, Tokyo, Japan) or the Leica TCS SP2 spectral confocal scanning system (Leica Microsystems, Wetzlar, Germany) with a 20 $\times$  objective lens, and images were acquired with Leica Confocal Software version 2.5.

**Measurement of EEA1-positive vesicles.** For analysis of early endosomes, the number of EEA1-positive vesicles in COS-7 cells expressing EGFP chimeras (and containing an intact nucleus stained with 4',6'-diamidino-2-phenylindole [DAPI]) was quantified with Image-Pro Plus software version 4.5.1 (Media Cybernetics, Silver Spring, MD). EEA1-positive vesicles ( $>0.04 \mu\text{m}^2$ ) were assayed by counting 40 cells. After we extracted the morphology of EEA1-positive endosomes with the object-extracting module of Image-Pro Plus, the clustered vesicles were separated with the Watershed Split module in the software. These data were statistically analyzed with Prism software version 3.0c (GraphPad, San Diego, CA). The data were statistically evaluated with one-way analysis of variance, followed by Bonferroni's test.

**Endocytosis.** Transferrin or Sulforhodamine 101 uptake was assessed as described previously (14, 50). Briefly, COS-7 cells were transfected with EGFP or EGFP-Solo constructs by using Lipofectamine 2000. Seven hours after transfection, the cells were depleted of bovine transferrin by incubation for 45 min in Dulbecco modified Eagle medium containing 0.1% bovine serum albumin and then labeled with human transferrin fluorescently labeled with Alexa-594 (Molecular Probes) at 25  $\mu\text{g}/\text{ml}$  or with the fluid-phase fluorescent marker Sulforhodamine 101 (Molecular Probes) at 25  $\mu\text{g}/\text{ml}$  for 15 min at 37°C. Internalization was then stopped by placing the cells on ice and washing them three times with ice-cold PBS before formaldehyde fixation. For analysis of endocytosis, fluorescence of Alexa-594-labeled transferrin or Sulforhodamine 101 in COS-7

cells expressing EGFP-Solo chimeras was quantified with Image-Pro Plus software version 4.5.1 with the density histogram module.

**Cortical neuron morphometry and analysis.** Images of immunostained neurons as described above were captured with an ORCA-ER digital camera, and morphometric analysis of the neurites and their branching was performed with Kurabo Neurocyte Image Analyzer software version 1.5 (KURABO, Osaka, Japan). To analyze the effects on neurite morphology, EGFP-positive cells were assayed by counting at least 60 cells from randomly selected fields. All neurites were measured irrespective of whether they were axons. Neuronal morphology was assessed according to four criteria, pass (number of branches), joint (number of branch points), total length (axon-and-dendrite length), and average maximum neurite length (axon length; Tau1 immunohistochemistry showed that the longest neurite of E16 mouse-derived embryonic cortical neurons was an axon; data not shown). The data were statistically evaluated by one-way analysis of variance, followed by Bonferroni's test.

**Organotypic slice culture.** The method used for slice culture has been described previously (49). In brief, C57BL/6J mice were decapitated and their brains were dissected and sliced in ice-cold HBSS with a vibratome. P11 cerebella were sliced coronally at a 200- $\mu$ m thickness. Slices were transferred onto Millicell-CM inserts (Millipore, Bedford, MA) and cultured at the air-medium interface in 5% CO<sub>2</sub> in air at 37°C. Cerebellar slices were cultured essentially as described before (48), in a medium which consisted of 15% heat-inactivated horse serum (Invitrogen), 25% Earle's balanced salt solution (Sigma), 60% Eagle's basal medium (Invitrogen), 5.6 g/liter glucose, 3 mM L-glutamine, 20 nM progesterone, 1 mM sodium pyruvate, 100 U/ml penicillin, 100  $\mu\text{g}/\text{ml}$  streptomycin, and Sigma I-1884 supplement (giving final concentrations of 5  $\mu\text{g}/\text{ml}$  insulin, 5  $\mu\text{g}/\text{ml}$  transferrin, and 5 ng/ml sodium selenite). At 1 day in vitro, cerebellar slices were transfected with small interfering RNA (siRNA).

**Transfection of siRNA.** We used siRNA to knock down Solo/Trio8 expression in cerebellar-slice cultures. A 21-oligonucleotide siRNA duplex was designed by the siDirect program (RNAi Co., Ltd., Tokyo, Japan). The siRNA oligonucleotide sequences that were used to target the C-terminal transmembrane domain in Solo/Trio8 (region, bp 5483 to 5505) were 5'-GACAAGCAUACGUUGA UUG-3' (sense) and 5'-AAUCAACGUAAUGCUUGUCAU-3' (antisense) and were synthesized by RNAi Co., Ltd. For the control, scrambled siRNA, silencer negative control no. 1 siRNA (proprietary sequence; Ambion, Austin, TX) was used. To confirm the siRNA effect, the EGFP-Solo plasmid and siRNA targeting Solo/Trio8, as well as a scrambled siRNA control, were cotransfected into COS-7 cells with Lipofectamine 2000 according to the manufacturer's instructions. After 24 h, significant siRNA-mediated suppression of Solo/Trio8 expression was detected by immunocytochemistry with anti-GFP monoclonal antibody 3E6 to estimate the fluorescence intensity of EGFP-expressing cells by fluorescence microscopy. For analysis of the inhibitory efficiency of siRNA, fluorescence signals in COS-7 cells expressing EGFP-Solo were quantified with Image-Pro Plus software version 4.5.1 with the density histogram module. To knock down endogenous Solo/Trio8 expression in Purkinje cells, at 1 day in vitro the siRNA was transfected into cerebellar slices with X-tremeGENE siRNA Transfection Reagent (Roche Applied Science) according to the manufacturer's instructions. In addition, scrambled siRNA no. 1 was transfected as a negative control. After 2 days, the slices were immunostained with anti-calbindin D28k as described below.

**Immunohistochemistry.** For Purkinje neuron morphometry, Purkinje cells were visualized by immunostaining with a mouse monoclonal antibody against calbindin D28k. The immunostaining method for brain slices has been described previously (48). Briefly, slices were fixed in 4% paraformaldehyde in PBS for 1 h at room temperature and washed three times with PBS. Slices were incubated with 10% normal goat serum in PBS containing 0.3% Triton X-100 for 1 h. Slices were then incubated overnight at 4°C with primary antibody diluted 1:500 in PBS containing 3% normal goat serum and 0.3% Triton X-100 and then washed three times with PBS. Slices were incubated with goat Alexa 488-conjugated secondary antibody diluted 1:200 in PBS containing 1% goat serum and 0.3% Triton X-100 for 1 h at room temperature and washed three times with PBS. Images of immunostained Purkinje neurons were captured with the Leica TCS SP2 spectral confocal scanning system (20 $\times$  objective lens), and morphometric analysis of the axons was performed with the Kurabo Neurocyte Image Analyzer as described above.

**Nucleotide sequence accession number.** The nucleotide sequence of mouse Solo/Trio8 has been deposited in the DDBJ nucleotide sequence database under accession number AB106872.

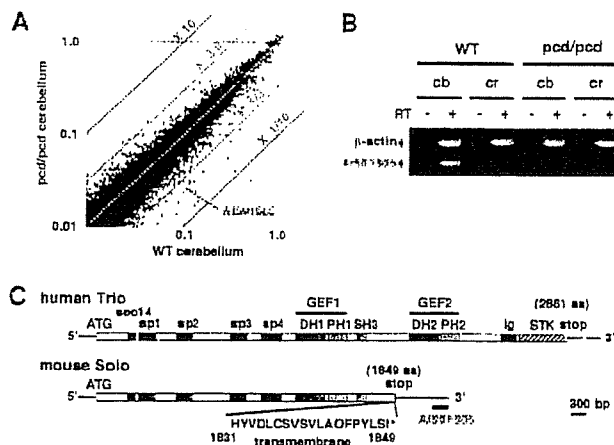


FIG. 1. Identification of a cDNA sequence predominantly expressed in Purkinje neurons. (A) Scattergram analysis of microarray data. Cerebellar cDNAs derived from pcd and WT mice were analyzed with DNA microarrays, and the average signal from each gene was normalized to the GAPDH signal and plotted to yield the scattergram. The AI591505 cDNA is indicated on the plot. (B) RT-PCR analysis of AI591505 transcript expression in the cerebella (cb) and cerebra (cr) of pcd and WT mice, respectively. PCRs for the  $\beta$ -actin gene (internal control) and AI591505 were performed in a single tube. (C) Structural relationship between the gene for Solo/Trio8 and a consensus of human Trio genes. Protein domains are indicated within the bars, and the 5' and 3' noncoding regions are indicated by horizontal lines. The domains shown are as follows: sec14, sec14p-like putative lipid binding domain; sp, spectrin-like domain; DH, Dbl homology domain; PH, pleckstrin homology domain; SH3, Src homology 3 domain; Ig, Ig-like domain; STK, serine/threonine kinase domain.

## RESULTS

**DNA microarray analysis of the pcd mouse cerebellum.** Since no exhaustive gene expression analysis of the pcd mouse has been reported to date, we evaluated changes in cerebellar gene expression from P24 pcd mice (with 70 to 80% Purkinje neuronal loss) and WT mice with DNA microarrays containing almost 6,000 characterized genes and 30,000 ESTs. A comparison between two pcd mice and two WT mice revealed pcd-specific variability in gene expression (Fig. 1A). A scattergram constructed from hybridization data of 12,518 highly expressed genes (those having signals  $>0.01\%$  of that measured for GAPDH) revealed only six upregulated genes ( $>3$ -fold) and 26 downregulated genes ( $<0.33$ -fold) in pcd mice (Table 1).

EST AI591505 is expressed exclusively in Purkinje neurons. Among the downregulated genes, we identified uncharacterized EST clone AI591505 (GenBank) (Fig. 1A; Table 1). AI591505 is 236 bp in length and has no homology with any annotated genes. The as-yet-uncharacterized AI591505 transcript was highly expressed in the normal mouse cerebellum ( $\sim 10\%$  of the GAPDH signal in the WT array; Fig. 1A). AI591505 was of interest because its decreased expression level in the pcd cerebellum suggested that it is a relatively highly expressed uncharacterized Purkinje neuron-specific gene. The decreased expression of the AI591505 transcript in the pcd cerebellum was confirmed by RT-PCR analysis with the cerebra and cerebella of pcd and WT mice, respectively. This transcript was expressed predominantly in the cerebellum, and expression in the pcd mouse was clearly lower than in the WT

mouse (Fig. 1B). In situ hybridization showed that the transcript was expressed predominantly in the WT Purkinje cell layer at P24 (Fig. 2B) but not in the E16 brain (Fig. 2A) and was decreased in pcd Purkinje cells (Fig. 2B, c to i). Relatively low-level expression was also detected in the olfactory bulb and hippocampus (Fig. 2B, c to e). The expression level of the AI591505 gene in the P7 pcd cerebellum (before onset of degenerative loss of Purkinje neurons) was equivalent to that in the P7 WT cerebellum (data not shown), although the *Nna1* (pcd causative gene) expression level was significantly decreased in the P7 pcd cerebellum (data not shown), suggesting that the AI591505 gene is not a downstream gene directly controlled by *Nna1* expression.

Identification of Solo/Trio8, a Trio splice variant, expressed predominantly in Purkinje neurons. An additional search of databases identified another EST, AI587721, containing a region overlapping the AI591505 sequence. 5' RACE with the AI587721 sequence yielded a 1.2-kbp cDNA clone from the cerebellum. A search of GenBank revealed that this clone contained a part of the *Trio* sequence (accession no. NM\_007118). To clone the entire ORF, a PCR was performed with primers for *Trio* (forward) and the cDNA clone (reverse)

TABLE 1. Genes with altered expression in the pcd cerebellum

Gene (accession no.)	Relative expression		pcd/WT ratio
	WT <sup>a</sup>	pcd <sup>a</sup>	
Genes upregulated in pcd cerebellum			
CPP32 (U63720)	0.042	0.137	3.29
TYRO (AF024637)	0.027	0.088	3.25
Slp-w7 (X06454)	0.024	0.082	3.45
UN <sup>b</sup> (AK084804)	0.015	0.046	3.08
UN <sup>b</sup> (BC055829)	0.014	0.043	3.00
DnaJ-like (AK053156)	0.011	0.036	3.37
Genes downregulated in pcd cerebellum			
IP3R1 (X15373)	0.533	0.054	0.10
28-kDa calbindin (D26352)	0.525	0.032	0.06
NK6 (AK083449)	0.396	0.113	0.29
PCP-1 (M21530)	0.356	0.040	0.11
RGS8 (AK044337)	0.322	0.084	0.26
GluR1 (BC056397)	0.299	0.098	0.33
PCP-2 (M21532)	0.298	0.056	0.19
DRR1-like (AK032875)	0.162	0.040	0.24
Ca <sup>2+</sup> -ATPase (BC026147)	0.146	0.019	0.13
PKC- $\gamma$ (L28035)	0.135	0.024	0.18
EAAC4 (D83262)	0.131	0.017	0.13
MGF (M57647)	0.129	0.031	0.24
Delphilin (AF099933)	0.127	0.013	0.10
rp S18a (AB049953)	0.114	0.031	0.27
AI591505	0.094	0.028	0.30
Tubulin ligase (AB093278)	0.087	0.014	0.16
Metalloprotease (AK034528)	0.074	0.023	0.31
Shank2 (AB099695)	0.066	0.019	0.28
PH protein (AK028383)	0.060	0.013	0.22
NSC dendrite regulator (BC030853)	0.056	0.017	0.31
Aspartate- $\beta$ -hydroxylase (AF289488)	0.056	0.017	0.31
Ca <sup>2+</sup> channel $\alpha 1G$ (AJ012569)	0.055	0.011	0.20
Tm4sf10 (BC019751)	0.049	0.015	0.31
Chemokine (AY241872)	0.039	0.013	0.32
Oxytocin-neurophysin I (M88355)	0.038	0.011	0.28
ARM repeat protein (AK044219)	0.033	0.010	0.30

<sup>a</sup> Expression level relative to GAPDH (average from two WT or pcd mice).

<sup>b</sup> UN: uncharacterized gene.

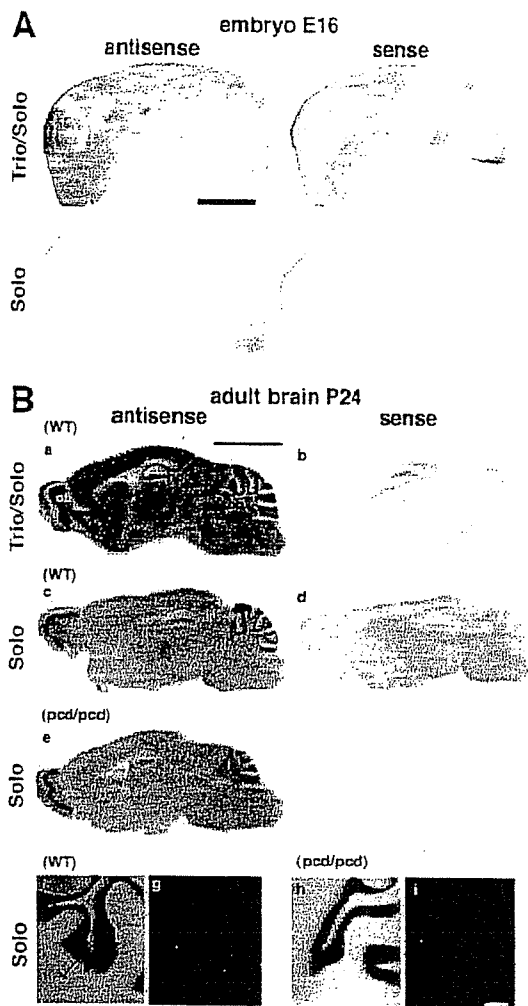


FIG. 2. Expression of Solo and Trio mRNAs in the mouse embryo and adult mouse brain. (A) In situ hybridization analysis of the mouse embryo (E16) with Solo-specific and Solo/Trio-common cRNA probes. Antisense and sense probes were prepared with Solo-specific and Solo/Trio (common to both) regions of the cDNA, respectively, and hybridized with tissue sections from an E16 mouse whole embryo. Bar = 5 mm. (B) In situ hybridization analysis of Solo transcript (AI591505) in P24 WT (a to d, f, g) and *pcd* (e, h, i) brains. Antisense and sense probes were prepared from Solo-specific and Solo/Trio (common to both) regions of the cDNA, respectively, and hybridized with tissue sections from P24 mouse whole brains. Regions in part a are labeled as follows: cb, cerebellum; ctx, cortex; hp, hippocampus; ob, olfactory bulb. The arrow in part f indicates the Purkinje cell layer, and the bars in part f indicate the molecular (lower) and granule (upper) layers. Bar in part a = 5 mm (same scale for parts a to e). Bar in part i = 200  $\mu$ m (same scale for parts f to i).

to yield a cDNA with an entire ORF of 5,550 bp encoding 1,849 aa (Fig. 1C) from the cerebellum. The human *Trio* ORF contains 8,586 bp encoding 2,861 aa (6) (Fig. 1C); the cloned cDNA lacked the region between nucleotides 5491 and 8586 but contained a distinct 874-bp sequence at the 3' end (Fig. 1C). A search of GenBank revealed the corresponding exon in the mouse *Trio* gene (data not shown), suggesting that the transcript is an alternatively spliced product of the *Trio* gene. We thus named this isoform Solo, for short-form splice variant

of *Trio*. Solo contains an N-terminal sec14-like domain, spectrin-like repeats, a GEF1 domain, one SH3-like domain, and the unique C-terminal hydrophobic sequence HYVDLCSVS VLAQFPYLSI (aa 1831 to 1849, Fig. 1C). Computational analyses with a protein motif search program (<http://motif.genome.ad.jp/>) suggested that this C-terminal hydrophobic sequence resembles transmembrane helices of G-protein-coupled receptors (data not shown). McPherson et al. recently reported identification of rat *Trio* variants (25). Among them, the amino acid sequence of rat *Trio8* was highly similar (99.7%) to that of mouse Solo, suggesting that Solo is a mouse homologue of *Trio8*.

To delineate the expression patterns of the genes for Solo/*Trio8* and *Trio* in the mouse brain, we performed in situ hybridization with Solo-specific and Solo/*Trio*-common cRNA probes. The Solo/*Trio*-common probe signal was distributed over the entire mouse brain, and more-intense signals were observed in the hippocampus, olfactory bulb, cortical layers, and cerebellum (Fig. 2B, a and b). This hybridization pattern differed from that of the Solo-specific probe, which was predominantly expressed in the Purkinje cell layer of the cerebellum (Fig. 2B, c, d, f, and g). To determine if Solo/*Trio8* mRNA is actually translated into protein, we performed Western blot analysis with a polyclonal antibody recognizing a 14-aa internal sequence near the N terminus of Solo and *Trio* (anti-Solo/*Trio* antibody). The immunoblot showed a 210-kDa immunoreactive band in the mouse cerebellum, in good agreement with the expected molecular mass of Solo (212 kDa) (data not shown). McPherson et al. (25) also detected a 210-kDa rat *Trio8* protein in the rat cerebellum by Western blotting with an antibody against *Trio8*. The size of the Solo/*Trio8* protein in mouse and rat cerebella was identical to that measured in COS-7 cells transfected with the Solo expression vector (Fig. 3C). Our antibody against Solo/*Trio* did not work well in immunohistochemical, immunocytochemical, and fractionation experiments (data not shown), so we were unable to determine the protein expression pattern in the brain.

**Guanine nucleotide exchange activity of Solo/*Trio8* for a Rho family GTPase.** The GEF1 domain of *Trio* activates RhoG and Rac1, whereas GEF2 acts on RhoA (3). We addressed whether the GEF1 domain of Solo/*Trio8* has guanine nucleotide exchange activity for Rac1 by a pull-down assay with the PBD of PAK1, which specifically binds to GTP-bound Rac1 (active form) but not to the inactive GDP-bound form (4). The amount of activated Rac1 in COS-7 cells transfected with the EGFP-Solo construct was markedly increased compared with that in negative control cells transfected with EGFP (Fig. 3B, top). Previous studies demonstrated that a double amino acid mutant form of *Trio* (Q1368A and L1376E within the GEF1 domain) completely abolishes the GEF1 activity (10, 23). The Q1368A and L1376E double mutation (EGFP-Solo-AE, Fig. 3A) abolished EGFP-Solo-mediated Rac1 activation in COS-7 cells (Fig. 3B, top). The C-terminal hydrophobic sequence (HYVDLCSVS VLAQFPYLSI; Fig. 1C) of Solo/*Trio8* was predicted by a protein motif search program to function as a membrane-anchoring domain (data not shown). Deletion of this putative domain (EGFP-Solo-TM(-), Fig. 3A) did not affect Rac1 activation (Fig. 3B, top). There was no significant difference in the total amount of Rac1 expressed in COS-7 cells transfected with the EGFP, EGFP-Solo, EGFP-

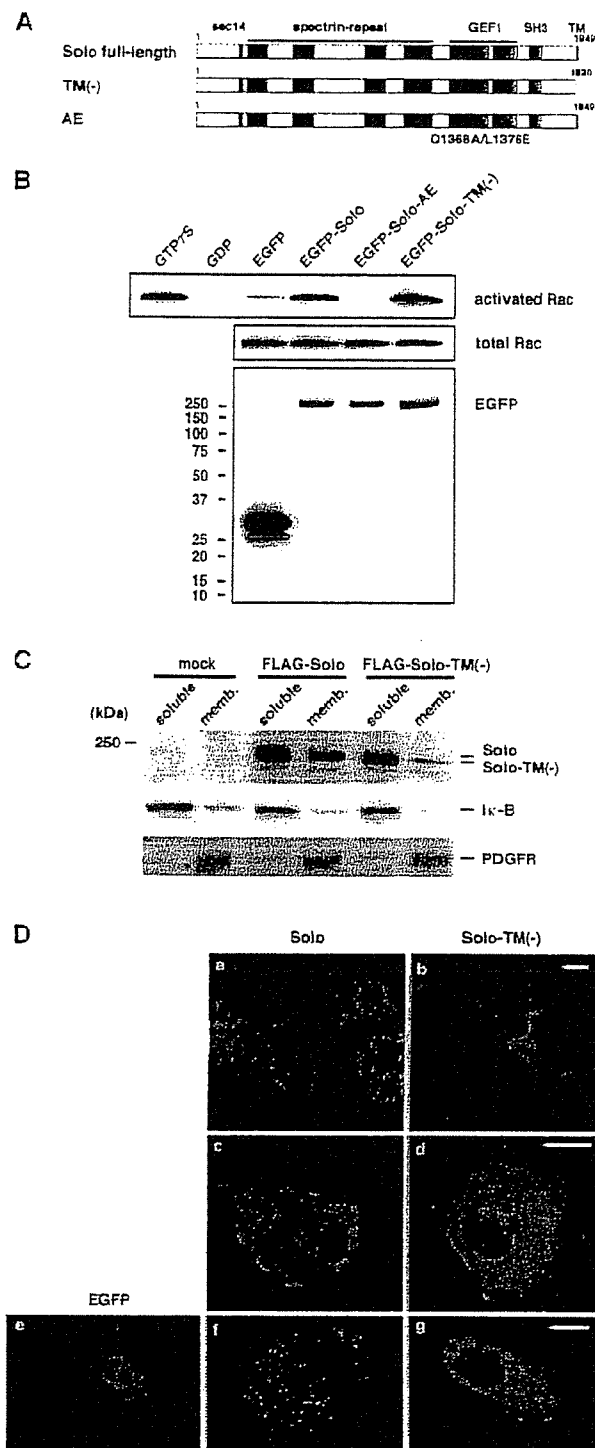


**FIG. 3.** GEF activity of Solo/Trio8 and localization in cellular membranes. (A) Schematic representation of full-length, C-terminally truncated Solo-TM(-) and AE mutant (GEF inactive; Q1368A/L1376E). (B) Rac1 activation by the GEF1 activity of Solo/Trio8. EGFP, EGFP-Solo, EGFP-Solo-AE, and EGFP-Solo-TM(-) were transiently expressed in COS-7 cells. Cells were cultured for 24 h and then serum starved for an additional 5 h prior to the Rac1 activation assay. PBD-bound Rac1 protein was pulled down and analyzed by Western blotting with monoclonal anti-Rac1. (Top) GTP-bound Rac1 (active form). Cell lysates treated with GTPγS or GDP served as

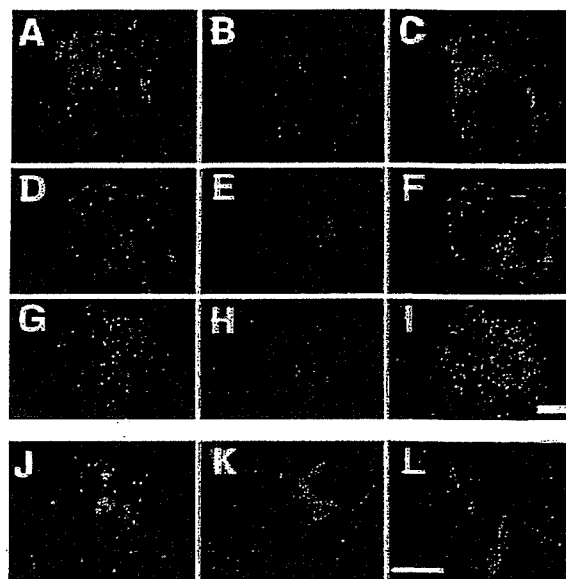


**FIG. 4.** Subcellular localization of Solo/Trio8. An EGFP-tagged Solo/Trio8 expression construct (green) was transfected into COS-7 cells (A, D, and G). COS-7 cells were further stained (red) with anti-Bip/GRP78 (B), anti-GM130 (E), or anti-EEA1 (H). Merged images are indicated to the right in each row (C, F, and I). Images were obtained by confocal microscopy. The EGFP-tagged Solo/Trio8 expression construct was transfected into 293 cells, and EGFP staining (green) was assessed. The 293 cells were further stained (red) for specific markers with anti-Rab5a (J), anti-Rab7 (K), or anti-Rab11 (L). Merged images are indicated, and colocalization is shown in yellow (blue arrowheads in J). Images were obtained with a charge-coupled device camera. Bars = 5 μm.

Solo-AE, or EGFP-Solo-TM(-) expression construct (Fig. 3B, middle). Furthermore, the amount of EGFP-Solo did not differ between COS-7 cells transfected with WT or mutant Solo constructs (Fig. 3B, bottom).

**Solo/Trio8 localizes to early endosomes.** To address whether the potential C-terminal membrane-anchoring domain of Solo/Trio8 is required for membrane association, N-terminally FLAG-tagged Solo and Solo-TM(-) expression constructs (Fig. 3A) were transfected into COS-7 cells and the cell lysates

the respective positive and negative controls. (Middle) Total cell lysates probed for Rac1 demonstrate equal amounts of total Rac1 in all transfected cells. (Bottom) Expression of transfected proteins was evaluated by Western blotting with anti-GFP. The values on the left are molecular sizes in kilodaltons. (C) COS-7 cells were transfected with pCI-neo (mock), pCI-neo-FLAG-Solo, or pCI-neo-FLAG-Solo-TM(-). Soluble and membrane proteins were subjected to sodium dodecyl sulfate-polyacrylamide gel electrophoresis and immunoblotted with anti-FLAG, anti-Iκ-B (soluble-protein control), or anti-PDGFRα/β (membrane protein control). (D) Fluorescence microscopy of cells transfected with N- or C-terminally EGFP- or FLAG-tagged Solo or C-terminally truncated Solo-TM(-) expression constructs. Expression constructs encoding N-terminally EGFP-tagged Solo and Solo-TM(-) were transfected into COS-7 cells (a, b). Expression constructs of C-terminally FLAG-tagged Solo and Solo-TM(-) were transfected into COS-7 cells and stained with anti-FLAG (c, d). EGFP alone, C-terminally EGFP-tagged Solo, and Solo-TM(-) mutant expression constructs were transfected into NIH 3T3 cells (e to g). Bars = 10 μm.

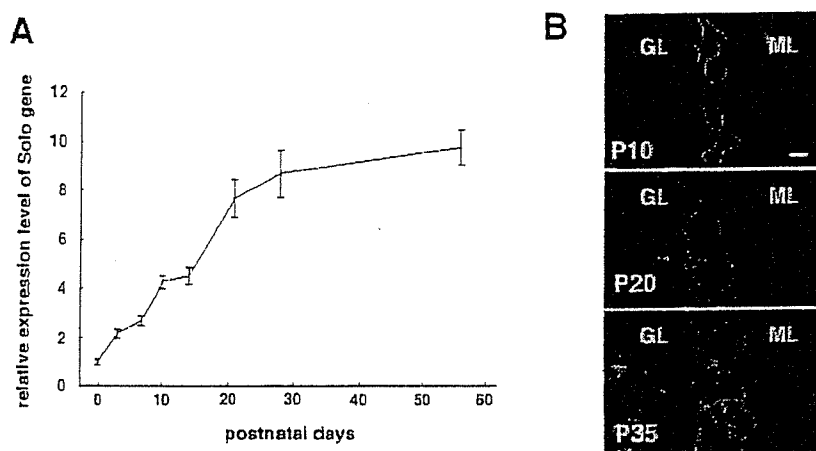


FIG. 5. Expression profile of Solo/Trio8 and the increase in the number of early endosomes during postnatal mouse cerebellar development. (A) SYBR green-based quantitative RT-PCR analysis of Solo/Trio8 transcript in WT mouse cerebellum during postnatal development. Expression levels are relative to P0 (P0 = 1.0). Each bar represents the mean  $\pm$  the standard error of the mean ( $n = 3$ ; three cerebella). (B) Immunohistochemistry of cerebellum sections during stages of postnatal maturation of Purkinje neurons (P10, P20, and P35). A section (20  $\mu$ m) was obtained from a C57BL/6J mouse brain. Sections were stained with anti-calbindin and coimmunostained with anti-EEA1. Merged images are shown in gray. Green lines indicate the location of each cell body of calbindin-positive Purkinje neurons. Bright, dot-like signals indicate EEA1-positive early endosomes. GL, granule cell layer; ML, molecular cell layer. Bar = 20  $\mu$ m

were analyzed by Western blotting. N-terminally FLAG-tagged Solo was a single band of  $\sim$ 220 kDa that localized to both soluble and membrane fractions (Fig. 3C). Nearly all of the N-terminally FLAG-tagged Solo-TM(–) was found in the soluble fraction (Fig. 3C), indicating that the C-terminal domain is essential for membrane anchoring. The internal control proteins I $\kappa$ B (soluble) and PDGF receptor  $\alpha/\beta$  (membrane associated) were detected in the appropriate fractions (Fig. 3C). The subcellular localization of Solo was confirmed by immunofluorescence microscopy of N- or C-terminally EGFP- or FLAG-tagged Solo constructs. The N-terminally tagged construct displayed a pattern consistent with localization to the cytoplasm and to small vesicles in COS-7 cells (Fig. 3D, a; Fig. 4A, D, and G), 293 cells (Fig. 4J to L), and primary cultured neurons (see Fig. 7D). The C-terminally tagged protein yielded similar results (Fig. 3D, c, COS-7; Fig. 3D, f, NIH 3T3). N-terminally and C-terminally EGFP- or FLAG-tagged Solo-TM(–) displayed uniform cytoplasmic localization (Fig. 3D, b, d, and g). These results indicated that the putative C-terminal membrane-anchoring domain is essential for vesicular localization. Although various N-terminally truncated Solo mutant constructs generated by serial deletion of N-terminal domains, including the sec14-like and spectrin-repeat domains, also failed to distribute to vesicles, Western blotting revealed that these mutant proteins were not stable in COS-7 cells (data not shown).

Subcellular localization of Solo/Trio8 was then analyzed with organelle-specific markers. Antibodies against Bip/GRP78, GM130, and EEA1 specifically label the endoplasmic reticulum (22, 31), Golgi (1), and early endosomes (5, 9), respectively (Fig. 4B, E, and H). Of these markers, only the signal for the early-endosome marker EEA1 partially overlapped the EGFP-Solo signal (Fig. 4A to I), suggesting that Solo/Trio8 localizes to early endosomes. To confirm the localization with other endosomal markers and another cell type, we stained EGFP-Solo-expressing 293 cells with specific anti-

bodies to Rab5 for early endosomes (28), Rab7 for late endosomes (11), and Rab11 for recycling endosomes (40). EGFP-Solo staining partially overlapped Rab5-positive vesicles (Fig. 4J) but not Rab7- or Rab11-positive vesicles (Fig. 4K and L). These data indicated that Solo/Trio8 localizes to early endosomes. However, at this level of resolution, we could not rule out the possibility that the observed colocalization of Solo with EEA1 and Rab5 arose from coincidental overlap due to the high-density punctate staining resulting from overexpression of these proteins.

We could not define which subclass of early endosomes expressed Solo/Trio8 because specific markers for such a classification are not available.

**Solo/Trio8 gene expression correlates with early-endosome maturation levels in postnatal Purkinje neuronal cells.** We analyzed the temporal pattern of the Solo/Trio8 gene expression level during Purkinje neuron maturation after birth (Fig. 5A). Analysis of mRNA samples prepared from P0 to P56 cerebella showed that the gene for Solo/Trio8 was expressed after birth, markedly increased during the first 4 weeks of life, and achieved maximal levels during adulthood. To investigate the development of early endosomes in Purkinje neurons, we stained cerebellar brain sections with antibodies against EEA1 and calbindin D28k (Purkinje neuron marker) (34). The number of large EEA1-positive early endosomes increased in Purkinje neurons during the postnatal maturation stage after P20 (Fig. 5B), indicating a correlation between expression levels of Solo/Trio8 and early-endosome development in D28k-positive Purkinje neurons.

**Solo/Trio8 modulates early-endosome dynamics via its GEF1 activity and C-terminal membrane-anchoring domain.** We assessed the effect of Solo overexpression on EEA1-positive early endosomes in COS-7 cells. The average number of EEA1-positive early endosomes increased in EGFP-Solo-expressing cells (1.84-fold  $\pm$  0.217-fold versus EGFP alone;  $P < 0.001$ ,  $n = 40$ ; Fig. 6A and B). We next addressed whether

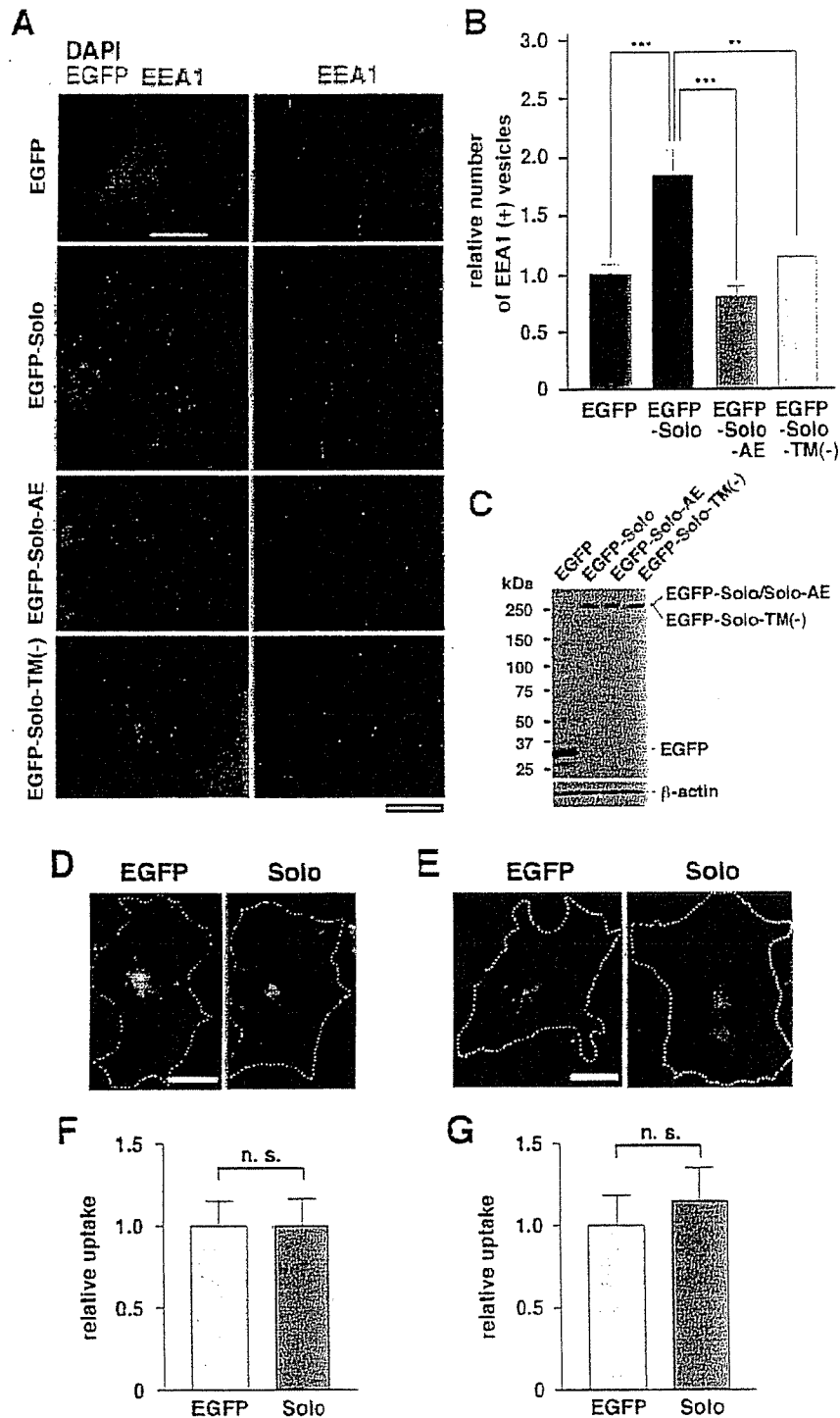


FIG. 6. Solo/Trio8 modulates early-endosome dynamics. (A) Expression constructs of the control EGFP, EGFP-Solo, EGFP-Solo-AE (GEF1 inactive form), and EGFP-Solo-TM(-) were transfected into COS-7 cells (EGFP signal is indicated in green). At 8 h posttransfection, cells were stained with anti-EEA1 (red) and DAPI (blue). Merged tricolor images are shown to the left. For ease of visualization, two-color images (minus the green EGFP signal) are shown to the right. Dotted lines indicate cellular edges. Images were obtained with a cooled charge-coupled device camera. Bars = 10  $\mu$ m. (B) Quantification of EEA1-positive vesicles (early endosomes; survey square,  $>0.04 \mu\text{m}^2$ ) in COS-7 cells transfected with Solo/Trio8 expression constructs. The number of early endosomes counted for each construct is presented relative to that determined for EGFP-expressing cells (negative control; EGFP = 1.0). Each bar represents the mean  $\pm$  the standard error of the mean ( $n = 40$  cells for each construct). \*\*,  $P < 0.01$ ; \*\*\*,  $P < 0.001$ . (C) Protein expression levels of EGFP (negative control), EGFP-Solo, EGFP-Solo-AE, and EGFP-Solo-TM(-) constructs were analyzed by Western blotting (8  $\mu$ g protein per lane) with anti-Living Colors A.v. for EGFP detection.  $\beta$ -Actin expression was monitored as an internal control. (D to G) Effect of Solo/Trio8 on endocytosis. COS-7 cells expressing EGFP or EGFP-Solo were

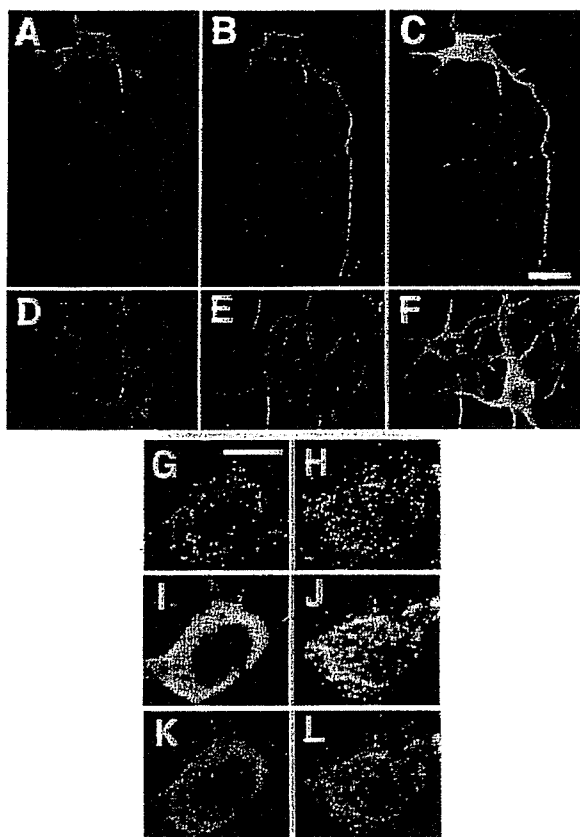


FIG. 7. Subcellular localization of Solo/Trio8 in cultured cortical neurons transfected with the EGFP-tagged Solo expression construct. EGFP signal (green) was observed in axons (A) and dendrites (D). These same cells were stained with anti-Tau1 (B) and anti-Map2 (E). Merged images are indicated to the right in each row (C and F). Images were obtained by confocal microscopy. Bar in panel C = 20  $\mu$ m (same scale for panels A to F). (G to L) Cultured cortical neurons transfected with the EGFP (I) or EGFP-tagged Solo (J) expression construct. These same cells were stained with anti-Rab5a (G and H). Merged images are indicated in the lower panels (K, EGFP and Rab5a; L, EGFP-Solo and Rab5a). Bar in panel G = 10  $\mu$ m (same scale for panels G to L).

GEF1 activity is required to induce the increase in EEA1-positive early endosomes with the double mutant Solo-AE (Fig. 3A), which lacks guanine nucleotide exchange activity for Rac1 (Fig. 3B). The endosome-inducing activity of this mutant was compared with that of EGFP-Solo. As expected, expression of EGFP-Solo-AE did not increase the number of EEA1-positive early endosomes (Fig. 6A and B). However, the lack of GEF1 activity altered the early-endosomal location of Solo/Trio8 (Fig. 6A). On the other hand, the distribution pattern of Solo-AE resembled that expected for lysosomal membranes,

suggesting that the GEF1 activity is involved in selective transfer of Solo/Trio8 from early endosomes to late endosomes-lysosomes. Given that the Solo membrane-anchoring domain is required for membrane localization (Fig. 3C and D), we further addressed whether this domain is required to induce an increase in the number of EEA1-positive endosomes. The truncated mutant Solo-TM(-) did not increase the number of EEA1-positive endosomes (Fig. 6A and B). On the other hand, EGFP-Solo did not significantly affect the size of individual EEA1-positive early endosomes relative to EGFP-Solo mutants (data not shown). Western blotting and immunofluorescence microscopy of EGFP-derived signals in COS-7 cells confirmed that the expression levels and integrity of EGFP-Solo-AE and EGFP-Solo-TM(-) were similar to those of EGFP-Solo (Fig. 6A and C). To probe the mechanism of the Solo/Trio8-induced increase in early endosomes, we investigated the effect of Solo/Trio8 expression on endocytosis in COS-7 cells. The uptake of Alexa Fluor 594-labeled human transferrin and Sulforhodamine 101 did not change in EGFP-Solo-transfected COS-7 cells compared with control EGFP-transfected cells (Fig. 6D to G), suggesting that Solo/Trio8 modulates early-to-late or early-to-recycling endosome transfer rather than endocytosis.

Solo/Trio8 localizes in axons and somatodendrites in primary cultured neurons. The gene for Solo/Trio8 is expressed in Purkinje neurons (Fig. 2B). Mature neurons have two polarized subcellular compartments, namely, axons and somatodendrites. Epithelial cells, including neurons, have polarized endosomes, that is, apical (axonal) endosomes and basolateral (somatodendrite) endosomes (2). To assess whether Solo/Trio8 localizes to early endosomes in a cell polarity-dependent manner in neuronal cells, we analyzed the EGFP-Solo distribution in primary cultured neurons. EGFP-Solo localized to small, Rab5-positive vesicles in soma (Fig. 7G to L), indicating localization to early endosomes. Moreover, EGFP-Solo was detected both in Map2-positive dendrites and in Tau1-positive axons (Fig. 7A to F). These results indicated that Solo localizes to both axons and somatodendrites in a cell polarity-independent manner.

Solo/Trio8 promotes neurite elongation in primary cultured neurons. Since endosomal membrane trafficking in neurons is involved in the regulation of neurite morphology (16, 19, 33), we analyzed the effects of Solo/Trio8 on neurite morphology in primary cultured cortical neurons. The total neurite length (axon and dendrite length) of the cortical neurons transfected with the EGFP-Solo expression construct significantly increased (about twofold) compared with cells transfected with the negative control EGFP construct (EGFP versus EGFP-Solo =  $718.1 \pm 66.8 \mu$ m versus  $1,321.0 \pm 111.4 \mu$ m;  $n = 74$  and  $97$  neurons, respectively;  $P < 0.01$ ; Fig. 8A and D). The EGFP-Solo expression construct also significantly increased (about twofold) the average maximal axon length in the primary cul-

incubated with Alexa 594-conjugated transferrin (25  $\mu$ g/ml; D) or Sulforhodamine 101 (25  $\mu$ g/ml; E) for 15 min and then fixed. Internalized transferrin or sulforhodamine (F and G) after 15 min of uptake was quantified by measuring the fluorescence intensity per cell as detected in panels D and E. The uptake of fluorescence for each construct is presented relative to that for EGFP-expressing cells (negative control; EGFP = 1.0). Each bar represents the mean  $\pm$  the standard error of the mean ( $n > 10$  cells for each construct). The differences in uptake between EGFP- and EGFP-Solo-expressing COS-7 cells were not significant (n.s.). Scale bars = 10  $\mu$ m.

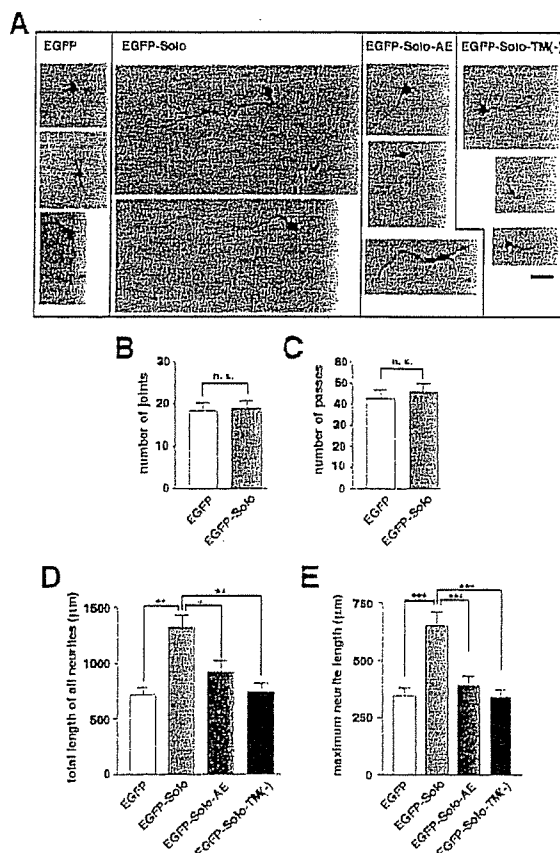


FIG. 8. Effects of Solo/Trio8 on neurite elongation in cultured cortical neurons. (A) Morphology of EGFP-Solo- or EGFP-Solo mutant-expressing neurons with anti-DsRed staining. Representative examples of fluorescence images (DsRed-derived signal; dark signals) of neurons transfected with control EGFP, EGFP-Solo, EGFP-Solo-AE, or EGFP-Solo-TM(-) constructs together with DsRed at 6 days in vitro are shown. To visualize the transfected neurons and their morphology, neurons were fixed and coimmunostained with anti-DsRed and anti-EGFP. Scale bar = 100  $\mu$ m. (B and C) Quantification of the effects of EGFP and EGFP-Solo expression on the number of joints (branch points) (B) and passes (branch number) (C) per neuron (EGFP,  $n = 74$ ; EGFP-Solo,  $n = 97$ ). n.s., no significant difference. (D and E) Quantification of the effects of EGFP, EGFP-Solo, EGFP-Solo-AE, and EGFP-Solo-TM(-) expression on neurite length (total neurite length per neuron, dendrite length plus axon length) (D) and average maximal neurite length (axon length per neuron) (E) [EGFP,  $n = 74$ ; EGFP-Solo,  $n = 97$ ; EGFP-Solo-AE,  $n = 60$ ; EGFP-Solo-TM(-),  $n = 91$ ]. Each bar represents the mean  $\pm$  the standard error of the mean. \*,  $P < 0.05$ ; \*\*,  $P < 0.01$ ; \*\*\*,  $P < 0.001$ .

tured neurons (EGFP versus EGFP-Solo =  $347.3 \pm 35.64 \mu$ m versus  $650.9 \pm 60.94 \mu$ m;  $n = 74$  and 97 neurons, respectively;  $P < 0.001$ ; Fig. 8E). Mutant Solo expression constructs EGFP-Solo-AE and EGFP-Solo-TM(-) failed to induce either total neurite length or maximal elongation (Fig. 8A, D, and E). The number of joints (branch points) and passes (branches) did not change significantly upon EGFP-Solo expression (Fig. 8B and C). We were unable to quantify the total number of early endosomes per neuron because the size and complexity of neurons relative to COS-7 cells (Fig. 6) precluded the detection of all early endosomes with sufficient resolution in a single

image. However, EGFP-Solo was distributed in a vesicle-like pattern (similar to that in COS-7 cells) in axons and dendrites of neurons (Fig. 7 and data not shown), and this pattern was altered upon expression of Solo-AE or Solo-TM(-) (data not shown), as observed in COS-7 cells (Fig. 6A).

Solo/Trio8 siRNA affects calbindin D28k-positive neurite length in the granule cell layer of the cerebellum. We attempted to knock down expression of the gene for Solo/Trio8 by RNA interference. To find an RNA sequence that would be effective, we prepared seven siRNAs with different Solo/Trio8-specific target recognition sequences that lacked homology to other sequences in the mouse genome. We then transfected each siRNA together with the EGFP-Solo expression construct into COS-7 cells. Transfection of the siRNA (region, bp 5483 to 5505) with a target sequence in the potential membrane-anchoring domain of Solo significantly reduced the level of Solo protein by  $\sim 25\%$  (Fig. 9B and C) compared with that of COS-7 cells transfected with negative control scrambled siRNA no. 1 (Fig. 9A and C), negative control siRNA no. 2 (purchased from Ambion), or no siRNA (data not shown). The Solo/Trio8-specific siRNA did not affect the level of EGFP in cells transfected with the EGFP expression construct compared with negative control siRNA (data not shown). To investigate the role of Solo/Trio8 in neurite morphology, we transfected the Solo/Trio8-specific siRNA or negative control scrambled siRNAs into cells of organotypic brain slices (44) by a liposome-based in vivo siRNA-transfer method (51) that we had previously established. We prepared coronally sliced P11 cerebellar slices and cut them into left and right halves (Fig. 9D). One of the halves was transfected with Solo/Trio8-specific siRNA, and the other half was transfected with negative control siRNA. We confirmed efficient incorporation of transfected Cy3-labeled control siRNA no. 1 into cells in the cerebellar slice by confocal laser scanning microscopy (data not shown). We fixed the slices 2 days after transfection and stained them with anti-calbindin D28k to specifically visualize the morphology of Purkinje neurons. The lengths of calbindin D28k-positive neurites (axons of Purkinje neurons) in the granule cell layer of slices transfected with Solo/Trio8 siRNA were significantly shorter (39.2%;  $n = 4$ ;  $P = 0.0039$ , Student's  $t$  test) than those of slices transfected with negative control siRNA no. 1 (Fig. 9E to I), suggesting that Solo/Trio8 is essential for neurite elongation or maintenance of Purkinje axon length. The neurite morphology of neurons transfected with negative control siRNA no. 1, siRNA no. 2, or EGFP siRNA (purchased from Ambion) was not changed compared with that of untransfected Purkinje neurons (data not shown).

## DISCUSSION

A number of early-endosome-specific proteins have been identified to date. Among them, EEA1, a specific effector of Rab5, binds to early-endosomal membranes (5, 45). This localization of EEA1 is mediated via its FYVE domain that interacts with phosphatidylinositol 3-phosphate, whose intracellular distribution is restricted primarily to early endosomes (21). In the present study, DNA microarray analysis of *pcd* mice led us to identify a mouse Trio splice variant, Solo/Trio8, which localizes to early endosomes. Although Solo/Trio8 is likely embedded in the endosomal membrane (Fig. 3, 4, 6, and



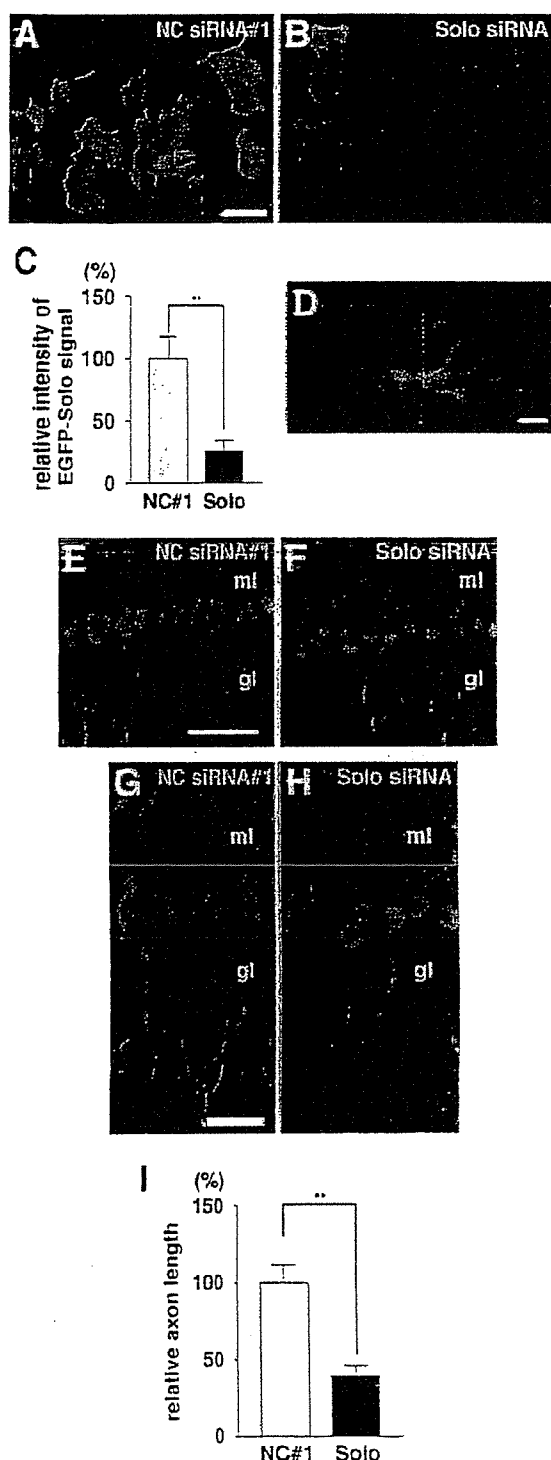


FIG. 9. Effects of Solo/Trio8 siRNA on Purkinje neurons. COS-7 cells were cotransfected with vectors encoding either EGFP-Solo and control scrambled siRNA (A, negative control [NC] siRNA no. 1) or EGFP-Solo and Solo/Trio8 siRNA (B, Solo siRNA) and then stained with anti-GFP (green) and DAPI (blue). (C) Effect of siRNA on EGFP-Solo expression quantified by measuring the fluorescence intensity per cell as detected in panels A and B. The effect of Solo siRNA on EGFP-Solo suppression is presented relative to that of negative control siRNA no. 1 (100%). Each bar represents the mean  $\pm$  the standard error of the mean ( $n > 10$  cells). Significant differences are

7), it does not contain a canonical FYVE-like motif. It is not clear which domain actively recruits Solo/Trio8 to early endosomes; however, an N-terminal region may be required for the recruitment since this region contains a sec14-like domain and spectrin-like repeats. Yeast Sec14 is a phosphatidylinositol transfer protein that catalyzes the exchange of phosphatidylinositol for phosphatidylcholine in membranes (43), suggesting that the sec14-like domain of Solo/Trio8 may function to link it to phosphatidylinositol 3-phosphate in early endosomes. The spectrin-like repeats constitute interaction sites for cytoskeletal and signal transduction proteins (8) and may facilitate the association of Solo/Trio8 (directly or indirectly) with early-endosome membranes. Cooperative interactions between the N- and C-terminal domains are likely to be important for targeting Solo to the early endosome and thus may represent a novel mechanism for protein localization to this organelle.

Solo/Trio8 mRNA expression was restricted to Purkinje neurons in the cerebellum and markedly increased during the maturation stage of these neurons after birth (Fig. 5A). EEA1-positive early-endosome signals also markedly increased in Purkinje neurons during this stage (Fig. 5B). We demonstrated that overexpression of Solo/Trio8 augmented the number of EEA1-positive early-endosomal vesicles in COS-7 cells, and the abrogation of Solo GEF1 activity attenuated this increase and disrupted the cellular distribution of early endosomes (Fig. 6). Taken together, these results suggest that Solo/Trio8 promotes postnatal maturation of the early-endosome pool in Purkinje neurons. Our data also suggest that Solo/Trio8 GEF1 activity is essential for the localization of this protein to early endosomes, and it may affect the maturation of the early-endosome pool directly via some small GTPases. The Trio GEF1 domain activates both Rac1 (Fig. 3B) and RhoG (3), and therefore Solo/Trio8 GEF1 may also activate downstream early-endosomal Rac1- or RhoG-type small GTPases. More than 150 small GTPases have been identified in the human genome, and the Rac1- and RhoG-type subfamily includes Rac1 to -3, RhoG, CDC42h, CDC42, TC10, and TCL (15). Among these, Rac1 and TC10 are present in endosomes (26, 27) but it is not known if either protein is a direct target for Solo/Trio8 GEF1 in early endosomes. Solo/Trio8 may activate multiple Rac1/RhoG-type small GTPases, each of which may

indicated by double asterisks ( $P < 0.01$ ;  $t$  test). Scale bar = 50  $\mu$ m. (D) Overview of a coronally sliced cerebellum. Scale bar = 1 mm. Cerebellar slices derived from P11 were cut into left and right halves (at the red dotted line). One of the halves was transfected with Solo/Trio8-specific siRNA (F and H; Solo siRNA), and the another half was transfected with negative control siRNA no. 1 (E and G) at 1 day in vitro and then cultured for 2 days. Slices were stained with anti-calbindin D28k (green), showing the morphology of Purkinje cells. Panels G and H are high-magnification images of panels E and F, respectively. gl, granule cell layer; ml, molecular cell layer. The scale bar in panel E is 100  $\mu$ m (E and F), and that in panel G is 50  $\mu$ m (G and H). (I) Quantitative representation of the effect of Solo/Trio8 siRNA on the axon length of Purkinje neurons in the granule cell layer. The relative axon length for Solo siRNA is presented relative to that for negative control siRNA no. 1 (100%). Each bar represents the mean  $\pm$  the standard error of the mean ( $n = 4$  slices). Significant differences are indicated by double asterisks ( $P < 0.01$ ;  $t$  test).

have a discrete function in early endosomes. Cellular Rac1 (26) had a distribution pattern distinct from that of Solo/Trio8, and Rac1 activation (Fig. 3) did not correlate with the increase in early endosomes induced by WT or mutant Solo/Trio8 (Fig. 6). Thus, Rac1 is unlikely to be the direct downstream target of Solo/Trio8. Identification of *in vivo* downstream targets for Solo/Trio8 may enhance our understanding of how Rho family GTPases regulate endosomal vesicle trafficking.

EGFP-Solo proteins were distributed in Tau1-positive axons, Map2-positive dendrites were distributed in cortical neurons (Fig. 7), and transfection of the EGFP-Solo construct induced both dendrite and axon elongation in these neurons (Fig. 8). These data indicate that Solo/Trio8 functions in a cell polarity-independent manner to regulate neuronal morphology. Furthermore, GEF1 activity and the C-terminal membrane-anchoring domain of Solo/Trio8 were essential for induction of not only neurite elongation but also of an increase in the number of early endosomes (Fig. 6 and 8). These equivalent domain requirements indicate that both biological activities are exhibited upon activation of early-endosome-associated Rho family GTPases, suggesting that Solo/Trio8 functions as an early-endosome-associated GEF to control cell polarity-independent neurite morphogenesis.

To date, two Trio family members, Trio and Kalirin, have been identified in mammals (3). The domain structure of Kalirin is nearly identical to that of Trio, and its expression is specific to the central nervous system (3). In addition, several short isoforms of Kalirin have been identified (18). Full-length Kalirin localizes to neuronal soma, where it displays a cytoplasmic protein-like diffuse immunostaining pattern. Interestingly, a Kalirin splice variant, Duo/Kalirin-7, lacking the C-terminal GEF2 and kinase domains (that is, a structure similar to that of Solo/Trio8) localizes to small punctate structures at neuronal processes and dendritic spines (18, 38). Duo/Kalirin-7 is involved in signal transduction during dendritic spine morphogenesis mediated by activation of the ephrinB receptor (37). We thus postulate that some of the cell surface receptors or adhesion molecules controlling neurite morphology are involved in Solo/Trio8-induced neurite elongation via the regulation of early-endosome dynamics.

Upstream effectors of endosome-specific Rab family small GTPases that localize to early endosomes have previously been characterized (39, 46). However, the activation mechanism of Rho family small GTPases that function in early endosomes is not well understood. Here, we identified Solo/Trio8 as a candidate upstream effector of Rho family GTPases that localize to early endosomes. The subcellular localization of Solo/Trio8 is mediated through a C-terminal membrane-anchoring domain and its GEF1 activity (Fig. 6A, EGFP-Solo-AE), and it is plausible that its endosomal localization may directly activate Rac1/RhoG-type small GTPases that sequentially modulate the dynamics of early endosomes. Our results show that Solo/Trio8 gene expression significantly increases during the postnatal maturation stage of Purkinje neurons in the cerebellum (Fig. 5). We also demonstrate that a Solo/Trio8-specific siRNA induces loss of calbindin D28k-positive neurite morphology in cultured cerebellar slices (Fig. 9). These data suggest that changes in early-endosome dynamics, as modulated by Solo, control neurite morphogenesis and/or maintenance of Purkinje neurons *in vivo*.

## ACKNOWLEDGMENTS

This work was supported by Grants-in-Aid for Scientific Research from the Ministry of Health, Labor and Welfare of Japan; Grants-in-Aid for Scientific Research from the Ministry of Education, Culture, Sports, Science and Technology of Japan; a grant from Pharmaceuticals and Medical Devices Agency; and a grant from the Japan Science and Technology Agency.

## REFERENCES

- Aoki, S., Q. Su, H. Li, K. Nishikawa, K. Ayukawa, Y. Hara, K. Namikawa, S. Kiryu-Seo, H. Kiyama, and K. Wada. 2002. Identification of an axotomy-induced glycosylated protein, AIGP1, possibly involved in cell death triggered by endoplasmic reticulum-Golgi stress. *J. Neurosci.* 22:10751-10760.
- Apodaca, G. 2001. Endocytic traffic in polarized epithelial cells: role of the actin and microtubule cytoskeleton. *Traffic* 2:149-159.
- Bateman, J., and D. Van Vactor. 2001. The Trio family of guanine-nucleotide-exchange factors: regulators of axon guidance. *J. Cell Sci.* 114:1973-1980.
- Benard, V., and G. M. Bokoch. 2002. Assay of Cdc42, Rac, and Rho GTPase activation by affinity methods. *Methods Enzymol.* 345:349-359.
- Christoforidis, S., H. M. McBride, R. D. Burgoyne, and M. Zerial. 1999. The Rab5 effector EEA1 is a core component of endosome docking. *Nature* 397:621-625.
- Debant, A., C. Serru-Pages, K. Seipel, S. O'Brien, M. Tang, S. H. Park, and M. Streuli. 1996. The multidomain protein Trio binds the LAR transmembrane tyrosine phosphatase, contains a protein kinase domain, and has separate rac-specific and rho-specific guanine nucleotide exchange factor domains. *Proc. Natl. Acad. Sci. USA* 93:5466-5471.
- Delcroix, J. D., J. S. Valletta, C. Wu, S. J. Hunt, A. S. Kowal, and W. C. Mobley. 2003. NGF signaling in sensory neurons: evidence that early endosomes carry NGF retrograde signals. *Neuron* 39:69-84.
- Djinovic-Carugo, K., M. Gautel, J. Ylanne, and P. Young. 2002. The spectrin repeat: a structural platform for cytoskeletal protein assemblies. *FEBS Lett.* 513:119-123.
- Dumas, J. J., E. Merithew, E. Sudharshan, D. Rajamani, S. Hayes, D. Lowe, S. Corvera, and D. G. Lambright. 2001. Multivalent endosome targeting by homodimeric EEA1. *Mol. Cell* 8:947-958.
- Estruch, S., S. Schmidt, S. Diriong, A. Penna, A. Blangy, P. Fort, and A. Debant. 2002. The human Rho-GEF trio and its target GTPase RhoG are involved in the NGF pathway, leading to neurite outgrowth. *Curr. Biol.* 12:307-312.
- Feng, Y., B. Press, and A. Wandinger-Ness. 1995. Rab 7: an important regulator of late endocytic membrane traffic. *J. Cell Biol.* 131:1435-1452.
- Fernandez-Gonzalez, A., A. R. La Spada, J. Treadaway, J. C. Higdon, B. S. Harris, R. L. Sidman, J. I. Morgan, and J. Zuo. 2002. Purkinje cell degeneration (pcd) phenotypes caused by mutations in the axotomy-induced gene, *Nna1*. *Science* 295:1904-1906.
- Gasman, S., Y. Kalaidzidis, and M. Zerial. 2003. RhoD regulates endosome dynamics through Diaphanous-related Formin and Src tyrosine kinase. *Nat. Cell Biol.* 5:195-204.
- Gomez, G. A., and J. L. Daniotti. 2005. H-Ras dynamically interacts with recycling endosomes in CHO-K1 cells: involvement of Rab5 and Rab11 in the trafficking of H-Ras to this pericentriolar endocytic compartment. *J. Biol. Chem.* 280:34997-35010.
- Heo, W. D., and T. Meyer. 2003. Switch-of-function mutants based on morphology classification of Ras superfamily small GTPases. *Cell* 113:315-328.
- Huang, E. J., H. Li, A. A. Tang, A. K. Wiggins, R. L. Neve, W. Zhong, L. Y. Jan, and Y. N. Jan. 2005. Targeted deletion of numb and numlike in sensory neurons reveals their essential functions in axon arborization. *Genes Dev.* 19:138-151.
- Jarrousse, N., and R. B. Kelly. 2001. Endocytotic mechanisms in synapses. *Curr. Opin. Cell Biol.* 13:461-469.
- Johnson, R. C., P. Penzes, B. A. Eipper, and R. E. Mains. 2000. Isoforms of kalirin, a neuronal Dbl family member, generated through use of different 5'- and 3'-ends along with an internal translational initiation site. *J. Biol. Chem.* 275:19324-19333.
- Kimura, K., A. Mizoguchi, and C. Ide. 2003. Regulation of growth cone extension by SNARE proteins. *J. Histochem. Cytochem.* 51:429-433.
- Kroschewski, R., A. Hall, and I. Mellman. 1999. Cdc42 controls secretory and endocytic transport to the basolateral plasma membrane of MDCK cells. *Nat. Cell Biol.* 1:8-13.
- Kutateladze, T., and M. Overduin. 2001. Structural mechanism of endosome docking by the FYVE domain. *Science* 291:1793-1796.
- Linnik, K. M., and H. Herscovitz. 1998. Multiple molecular chaperones interact with apolipoprotein B during its maturation. The network of endoplasmic reticulum-resident chaperones (ERp72, GRP94, calreticulin, and BiP) interacts with apolipoprotein b regardless of its lipidation state. *J. Biol. Chem.* 273:21368-21373.
- Liu, X., H. Wang, M. Eberstadt, A. Schnuchel, E. T. Olejniczak, R. P. Meadows, J. M. Schkeryantz, D. A. Janowick, J. E. Harlan, E. A. Harris, D. E. Staunton, and S. W. Fesik. 1998. NMR structure and mutagenesis of

- the N-terminal Dbl homology domain of the nucleotide exchange factor Trio. *Cell* 95:269–277.
24. Maeda, N., M. Niinobe, and K. Mikoshiba. 1990. A cerebellar Purkinje cell marker P400 protein is an inositol 1,4,5-trisphosphate (InsP3) receptor protein. Purification and characterization of InsP3 receptor complex. *EMBO J.* 9:61–67.
  25. McPherson, C. E., B. A. Eipper, and R. E. Mains. 2005. Multiple novel isoforms of Trio are expressed in the developing rat brain. *Gene* 347:125–135.
  26. Michaelson, D., J. Silletti, G. Murphy, P. D'Eustachio, M. Rush, and M. R. Phillips. 2001. Differential localization of Rho GTPases in live cells: regulation by hypervariable regions and RhoGDI binding. *J. Cell Biol.* 152:111–126.
  27. Miura, K., S. Miyazawa, S. Furuta, J. Mitsushita, K. Kamijo, H. Ishida, T. Miki, K. Suzukawa, J. Resau, T. D. Copeland, and T. Kamata. 2001. The Sos1-Rac1 signaling. Possible involvement of a vacuolar H<sup>+</sup>-ATPase E subunit. *J. Biol. Chem.* 276:46276–46283.
  28. Mohrmann, K., and P. van der Sluijs. 1999. Regulation of membrane transport through the endocytic pathway by rabGTPases. *Mol. Membr. Biol.* 16:81–87.
  29. Mukherjee, S., R. N. Ghosh, and F. R. Maxfield. 1997. Endocytosis. *Physiol. Rev.* 77:759–803.
  30. Mullen, R. J., E. M. Eicher, and R. L. Sidman. 1976. Purkinje cell degeneration, a new neurological mutation in the mouse. *Proc. Natl. Acad. Sci. USA* 73:208–212.
  31. Munro, S., and H. R. Pelham. 1986. An Hsp70-like protein in the ER: identity with the 78 kd glucose-regulated protein and immunoglobulin heavy chain binding protein. *Cell* 46:291–300.
  32. Nielsen, E., F. Severin, J. M. Backer, A. A. Hyman, and M. Zerial. 1999. Rab5 regulates motility of early endosomes on microtubules. *Nat. Cell Biol.* 1:376–382.
  33. Nishimura, T., Y. Fukata, K. Kato, T. Yamaguchi, Y. Matsuura, H. Kamiguchi, and K. Kaibuchi. 2003. CRMP-2 regulates polarized Numb-mediated endocytosis for axon growth. *Nat. Cell Biol.* 5:819–826.
  34. Nordquist, D. T., C. A. Kozak, and H. T. Orr. 1988. cDNA cloning and characterization of three genes uniquely expressed in cerebellum by Purkinje neurons. *J. Neurosci.* 8:4780–4789.
  35. O'Brien, S. P., K. Seipel, Q. G. Medley, R. Bronson, R. Segal, and M. Streuli. 2000. Skeletal muscle deformity and neuronal disorder in Trio exchange factor-deficient mouse embryos. *Proc. Natl. Acad. Sci. USA* 97:12074–12078.
  36. Otonari, A., S. Hadano, T. Okada, H. Mizumura, R. Kunita, H. Nishijima, J. Showguchi-Miyata, Y. Yanagisawa, E. Kohiki, E. Suga, M. Yasuda, H. Osuga, T. Nishimoto, S. Nurumiyu, and J. E. Ikeda. 2003. ALS2, a novel guanine nucleotide exchange factor for the small GTPase Rab5, is implicated in endosomal dynamics. *Hum. Mol. Genet.* 12:1671–1687.
  37. Penzes, P., A. Beaser, J. Chernoff, M. R. Schiller, B. A. Eipper, R. E. Mains, and R. L. Huganir. 2003. Rapid induction of dendritic spine morphogenesis by trans-synaptic ephrinB-EphB receptor activation of the Rho-GEF kalirin. *Neuron* 37:263–274.
  38. Penzes, P., R. C. Johnson, R. Sattler, X. Zhang, R. L. Huganir, V. Kumbhani, R. E. Mains, and B. A. Eipper. 2001. The neuronal Rho-GEF Kalirin-7 interacts with PDZ domain-containing proteins and regulates dendritic morphogenesis. *Neuron* 29:229–242.
  39. Pfeffer, S. 2003. Membrane domains in the secretory and endocytic pathways. *Cell* 112:507–517.
  40. Ren, M., G. Xu, J. Zeng, C. De Lemos-Chiarandini, M. Adesnik, and D. D. Sabatini. 1998. Hydrolysis of GTP on rab11 is required for the direct delivery of transferrin from the pericentriolar recycling compartment to the cell surface but not from sorting endosomes. *Proc. Natl. Acad. Sci. USA* 95:6187–6192.
  41. Rico, B., H. E. Beggs, D. Schahin-Reed, N. Kimes, A. Schmidt, and L. F. Reichardt. 2004. Control of axonal branching and synapse formation by focal adhesion kinase. *Nat. Neurosci.* 7:1059–1069.
  42. Schmidt, A., and A. Hall. 2002. Guanine nucleotide exchange factors for Rho GTPases: turning on the switch. *Genes Dev.* 16:1587–1609.
  43. Sha, B., S. E. Phillips, V. A. Bankaitis, and M. Luo. 1998. Crystal structure of the *Saccharomyces cerevisiae* phosphatidylinositol-transfer protein. *Nature* 391:506–510.
  44. Shima, Y., M. Kengaku, T. Hirano, M. Takeichi, and T. Uemura. 2004. Regulation of dendritic maintenance and growth by a mammalian 7-pass transmembrane cadherin. *Dev. Cell* 7:205–216.
  45. Simonsen, A., R. Lippe, S. Christoforidis, J. M. Gaullier, A. Brech, J. Callaghan, B. H. Toh, C. Murphy, M. Zerial, and H. Stenmark. 1998. EEA1 links PI(3)K function to Rab5 regulation of endosome fusion. *Nature* 394:494–498.
  46. Somsel Rodman, J., and A. Wandinger-Ness. 2000. Rab GTPases coordinate endocytosis. *J. Cell Sci.* 113(Pt. 2):183–192.
  47. Symons, M., and N. Rusk. 2003. Control of vesicular trafficking by rho GTPases. *Curr. Biol.* 13:R409–R418.
  48. Tanaka, M., N. Maeda, M. Noda, and T. Marunouchi. 2003. A chondroitin sulfate proteoglycan PTP $\zeta$ /RPTP $\beta$  regulates the morphogenesis of Purkinje cell dendrites in the developing cerebellum. *J. Neurosci.* 23:2804–2814.
  49. Tanaka, M., A. Tomita, S. Yoshida, M. Yano, and H. Shimizu. 1994. Observation of the highly organized development of granule cells in rat cerebellar organotypic cultures. *Brain Res.* 641:319–327.
  50. van der Luit, A. H., M. Buddé, P. Ruurs, M. Verheij, and W. J. van Blitterswijk. 2002. Alkyl-lysophospholipid accumulates in lipid rafts and induces apoptosis via raft-dependent endocytosis and inhibition of phosphatidylcholine synthesis. *J. Biol. Chem.* 277:39541–39547.
  51. Wang, Y. L., W. Liu, E. Wada, M. Murata, K. Wada, and I. Kanazawa. 2005. Clinico-pathological rescue of a model mouse of Huntington's disease by siRNA. *Neurosci. Res.* 53:241–249.

# Stargazin controls the pharmacology of AMPA receptor potentiators

Susumu Tomita<sup>\*†</sup>, Masayuki Sekiguchi<sup>‡</sup>, Keiji Wada<sup>‡</sup>, Roger A. Nicoll<sup>\*§¶</sup>, and David S. Bredt<sup>\*||</sup>

Departments of <sup>\*</sup>Physiology and <sup>§</sup>Cellular and Molecular Pharmacology, University of California, San Francisco, CA 94143; and <sup>‡</sup>Department of Degenerative Neurological Diseases, National Institute of Neuroscience, National Center of Neurology and Psychiatry, Kodaira, Tokyo 187-8502, Japan

Contributed by Roger A. Nicoll, April 19, 2006

Glutamate is the major excitatory neurotransmitter in brain, and  $\alpha$ -amino-3-hydroxy-5-methyl-4-isoxazolepropionic acid (AMPA)-type glutamate receptors (AMPA receptors) mediate the majority of postsynaptic depolarization. AMPAR ion channels display rapid gating, and their deactivation and desensitization determine the timing of synaptic transmission. AMPAR potentiators slow channel deactivation and desensitization, and these compounds represent exciting therapies for mental and neurodegenerative diseases. Previous studies showed that the AMPAR potentiators cyclothiazide and 4-[2-(phenylsulfonylamino)ethylthio]-2,6-difluorophenoxyacetamide display a preference for flip and flop alternatively spliced versions of glutamate receptor subunits, respectively. Here, we find that the AMPAR auxiliary subunit stargazin changes this pharmacology and makes both spliced forms of glutamate receptor subunit 1 sensitive to both classes of potentiator. Stargazin also enhances the effect of AMPAR potentiators on channel deactivation. This work demonstrates that stargazin controls AMPAR potentiator pharmacology, which has important implications for development of AMPAR potentiators as therapeutic agents.

transmembrane AMPA receptor regulatory protein | (TARP) | glutamate | synapse | psychiatry | cognition

Most excitatory transmission in brain occurs at synapses that use glutamate as the neurotransmitter. The  $\alpha$ -amino-3-hydroxy-5-methyl-4-isoxazolepropionic acid (AMPA)-type receptors (AMPA receptors) are glutamate-gated cation channels. Activation of these receptors provides most of the postsynaptic depolarization that induces neuronal firing. AMPAR channels show complex gating kinetics and vary considerably, depending on the subunit composition of the AMPAR (1). These channels open rapidly upon glutamate binding. The channels then desensitize quickly; that is, despite continued binding to agonist, the channels close with a desensitization time constant,  $\tau_{des}$ , of 1–15 ms. At most brain synapses, glutamate diffuses out of the cleft rapidly, even faster than AMPARs desensitize. The unbinding of glutamate from the receptor closes the channel, a process known as deactivation ( $\tau_{dea} \approx 1$ –3 ms). The timing of synaptic glutamate release and synaptic glutamate clearance interplays with AMPAR desensitization and deactivation. Collectively, these processes shape excitatory postsynaptic currents.

AMPA receptors are heterotetramers composed of glutamate receptor subunits 1–4 (GluR1–4) (2, 3). Each subunit can be alternatively spliced as either a “flip” (e.g., GluR1i) or a “flop” (e.g., GluR1o) version (4). This alternative splicing regulates channel kinetics, because the flop version desensitizes and deactivates more rapidly than does the flip version. In addition to the GluR pore-forming subunits, neuronal AMPARs also contain stargazin-like auxiliary subunits known as “transmembrane AMPAR regulatory proteins” (TARPs) (5). TARPs mediate AMPAR surface expression and synaptic clustering (5) and also modulate AMPAR channel gating by slowing desensitization and deactivation (6, 7).

AMPA potentiators are an exciting class of experimental therapeutics that promote AMPAR signaling by blunting desensitization and slowing deactivation (8). By promoting excitatory transmission, these agents show robust activity in a variety of

preclinical models. AMPAR potentiators enhance cognition, ameliorate depression, and lessen neurodegeneration in several animal models (8–13). In addition, AMPAR potentiators show discrete subunit specificity. The prototypical AMPAR potentiator, cyclothiazide, selectively potentiates responses of flip-type GluR subunits (14). On the other hand, the potentiator 4-[2-(phenylsulfonylamino)ethylthio]-2,6-difluorophenoxyacetamide (PEPA) acts specifically on flop isoforms (15). Here, we asked whether the stargazin subunit of AMPAR modulates the pharmacology of these potentiator drugs.

## Results

We used the *Xenopus laevis* oocyte expression system to evaluate stargazin effects on AMPAR function. As reported previously (6, 16), coinjection of stargazin cRNA increases glutamate-evoked currents from oocytes injected with GluR1i. To best compare the properties of channels containing GluR1 alone vs. GluR1 plus stargazin, we sought to study oocytes that had similar amounts of surface GluR1. We modulated surface receptor numbers by injecting oocytes with different amounts of stargazin and hemagglutinin epitope (HA)-GluR1i cRNA and quantified surface GluR1 by chemiluminescence as described in ref. 6. We found similar numbers of GluR1 surface receptors from oocytes injected with 0.5 ng of GluR1i alone and from those injected with 0.1 ng of GluR1i plus 0.1 ng of stargazin (Fig. 1A). As reported previously (6, 16), cyclothiazide greatly increased glutamate-evoked currents, both in oocytes injected with GluR1i alone and in those injected with GluR1i plus stargazin (Fig. 1A). Consistent with previous studies (14), we found that cyclothiazide has only modest effects on GluR1o expressed in oocytes (Fig. 1B). However, cyclothiazide greatly potentiated glutamate-evoked currents from oocytes expressing GluR1o plus stargazin (Fig. 1B). In the presence of stargazin, cyclothiazide increased steady-state currents in GluR1o-expressing oocytes by  $\approx 15$ -fold (Fig. 1B).

We performed analogous experiments exploring potentiation with PEPA, an AMPAR potentiator that preferentially affects flop receptors (15). As shown previously, we found that PEPA had minimal effects on GluR1i (Fig. 1C). In contrast, PEPA greatly increased currents from oocytes expressing GluR1i plus stargazin (Fig. 1C). As expected, GluR1o channels showed significant potentiation with PEPA; this potentiation was further increased by coinjection of GluR1o with stargazin.

To explore the effect of stargazin and AMPAR potentiators on channel desensitization and deactivation, we used a rapid perfusion

Conflict of interest statement: No conflicts declared.

Abbreviations: AMPA,  $\alpha$ -amino-3-hydroxy-5-methyl-4-isoxazolepropionic acid; AMPAR, AMPA receptor; GluR, glutamate receptor subunit; PEPA, 4-[2-(phenylsulfonylamino)ethylthio]-2,6-difluorophenoxyacetamide; TARP, transmembrane AMPAR regulatory protein; HA, hemagglutinin epitope.

<sup>†</sup>Present address: Department of Cellular and Molecular Physiology, Yale University School of Medicine, New Haven, CT 06520.

<sup>¶</sup>To whom correspondence may be addressed. E-mail: nicoll@cmp.ucsf.edu.

<sup>||</sup>To whom correspondence may be sent at the present address: Department of Integrative Biology, Eli Lilly and Company, Indianapolis, IN 46285. E-mail: bredt@lilly.com.

© 2006 by The National Academy of Sciences of the USA